Floquet wave–based analysis of transient scattering from doubly periodic, discretely planar, perfectly conducting structures

Nan-Wei Chen,[1,2] Mingyu Lu,[1] Filippo Capolino,[3] Balasubramaniam Shanker,[4] and Eric Michielssen[1]

Received 8 September 2004; revised 14 March 2005; accepted 12 April 2005; published 6 August 2005.

[1] A Floquet wave–based algorithm for solving an electric field time domain integral equation pertinent to the analysis of transient plane wave scattering from doubly periodic, discretely planar, perfect electrically conducting structures is presented. The proposed scheme accelerates the evaluation of fields generated by periodic constellations of band-limited transient currents via their expansion in time domain Floquet waves and use of blocked fast Fourier transforms. The validity and effectiveness of the resulting algorithm are demonstrated through a number of examples.

Citation: Chen, N.-W., M. Lu, F. Capolino, B. Shanker, and E. Michielssen (2005), Floquet wave–based analysis of transient scattering from doubly periodic, discretely planar, perfectly conducting structures, *Radio Sci.*, *40*, RS4007, doi:10.1029/2004RS003171.

1. Introduction

[2] This paper presents a marching-on-in-time (MOT) and Floquet wave–based scheme for solving an electric field time domain integral equation (TDIE) pertinent to the analysis of transient plane wave scattering from doubly periodic, perfect electrically conducting (PEC), discretely planar, and freestanding structures. The proposed approach uses blocked fast Fourier transform (FFT) based accelerators [*Harrier et al.*, 1985; *Bleszynski et al.*, 2001; *Yilmaz et al.*, 2002] to efficiently evaluate time domain Floquet wave (TDFW) decomposed electromagnetic fields [*Capolino and Felsen*, 2002, 2003; *Felsen and Capolino*, 2000; *Marrocco and Capolino*, 2002] generated by doubly periodic, discretely planar, and temporally band-limited source distributions.

[3] In the past, transient scattering from doubly periodic structures has been analyzed predominantly using finite difference time domain methods [*Veysoglu et al.*, 1993; *Tsay and Pozar*, 1993; *Harms and Mittra*, 1994; *Roden et al.*, 1998; *Holter and Steyskal*, 2002]. These solvers update fields inside a periodic structure's so-called mothercell using the classical Yee scheme [*Yee*, 1996] and impose periodic/absorbing boundary conditions on mothercell walls with normal vectors residing in/perpendicular to the plane of periodicity. Unfortunately, for obliquely excited periodic structures, these periodic boundary conditions call for future fields values to update current ones, and therefore cannot be applied directly. Several avenues for tackling this noncausality problem have been suggested [see *Maloney and Kesler*, 2002, and references therein]. It appears, however, that most fixes proposed to date are either hard to implement or somewhat limited in scope. Transient scattering from periodic structures also can be analyzed using TDIE-based schemes. Indeed, TDIE solvers for analyzing scattering from doubly periodic freestanding or substrate imprinted PEC elements were proposed by *Chen et al.* [2002, 2003]. Just like in their finite difference counterparts, noncausal terms arise when discretizing periodic structure TDIEs for obliquely incident fields using marching-on-in-time (MOT) procedures. *Chen et al.* [2002, 2003], removed these noncausal terms through the introduction of time-shifted temporal current basis functions in conjunction with a prolate-based extrapolation scheme. Unfortunately, even though these periodic structure TDIE solvers now efficiently cope with noncausal artifacts, their high computational complexity precludes them from being applied to the analysis of real-world structures. Generally speaking, the computational cost of MOT-based

[1]Department of Electrical and Computer Engineering, University of Illinois at Urbana-Champaign, Urbana, Illinois, USA.
[2]Now at Department of Electrical Engineering, National Central University, Chung-li, Taiwan.
[3]Dipartimento di Ingegneria dell'Informazione, Facoltà di Ingegneria, Università di Siena, Siena, Italy.
[4]Department of Electrical and Computer Engineering, Michigan State University, East Lansing, Michigan, USA.

0048-6604/05/2004RS003171

TDIE solvers can be attributed to their need to evaluate, at each and every time step, fields produced by past currents supported by the structure under analysis. The TDIE solvers of *Chen et al.* [2002, 2003] carry out this operation classically, by direct space-time convolution of the free space Green's function with all currents on the periodic structure. To be more specific, to evaluate the fields due to the past current, there is a double summation over the periodic cells. When the fields are observed on the mothercell, with the marching of time, the region around the mothercell in which the sources have to be take into account becomes larger and larger. This renders the solvers of *Chen et al.* [2002, 2003] computationally expensive.

[4] Here, an improved MOT-based TDIE solver for periodic structures is proposed. Whereas spectral methods for computing frequency domain Green's functions (Ewald representations [*Jordan et al.*, 1986], off-plane plane wave sums [*Jorgenson and Mittra*, 1991], etc.) are commonly used in periodic structure frequency domain integral equation solvers, the proposed solver is the first to do so within periodic structure TDIE simulators. The solver relies on a time domain Floquet wave (TDFW) representation of fields produced by periodic transient current constellations [*Capolino and Felsen*, 2002, 2003; *Felsen and Capolino*, 2000]. Specifically, the proposed solver exploits the fact that TDFW representations of fields produced by quiescent and band-limited sources only involve ''propagating modes'' (this fact, to the authors' knowledge demonstrated here for the first time for time domain signals, constitutes another important contribution of this paper). Hence TDFWs provide a natural, compact, and computationally efficient means of representing fields produced by band-limited sources residing on practical periodic structures that only support a finite and small number of propagating waves within their operating band, that is, structures with unit cells of linear dimensions on the order of the wavelength at the highest frequency in the incident field. Because the TDFW propagator is not time-local, costly time domain convolutions are carried out using a blocked-FFT scheme (first introduced in [*Harrier et al.*, 1985] for the purpose of solving one dimensional Volterra integral equations, and interpreted/tuned here within the proposed TDFW-TDIE framework). It will be shown that this decomposition and subsequent TDFW representation of the fields provides a means for computing fields produced by ''past'' currents in a manner consistent with the classical MOT-TDIE framework that is especially effective when the structure under study is discretely planar, viz. comprising a finite set of metallized layers. The computational cost of the new solver is only a fraction of that of periodic structure TDIE solvers not using TDFW concepts.

[5] This paper is organized as follows. Section 2 outlines the proposed TDFW/FFT-based scheme for rapidly computing transient fields produced by periodic current arrangements and its incorporation into an MOT-based TDIE solver for analyzing scattering from discretely planar structures. Section 3 presents numerical results that demonstrate the capability and accuracy of the proposed method. Section 4 relates our conclusions and avenues for future research.

2. Formulation

[6] Below, following a high-level description of the proposed solver, the periodic structure TDIE solver and TDFW concepts described by *Chen et al.* [2003] and *Capolino and Felsen* [2003] are reviewed. Next, the implementation of the proposed algorithm is outlined with emphasis placed on the FFT-based scheme for accelerating temporal convolutions involving TDFW kernels.

2.1. Outline of the Proposed Solver

[7] The proposed solver derives from a periodic structure TDIE solver developed earlier by several of the authors. The solver is accelerated by using a TDFW expansion of scattered fields and blocked-FFT methods. Below, these solver aspects are discussed in turn.

2.1.1. Periodic Structure TDIE Solver

[8] The periodic structure TDIE solver that forms the basis of the proposed simulator is almost identical to that of *Chen et al.* [2003]. When a periodic structure is excited by a transient plane wave, currents and fields in different cells are related to one another by a simple temporal shift. The TDIE solver considers as unknown the currents in one cell (the ''mothercell'') and imposes boundary conditions on the electric field throughout the same cell. To this end, the solver computes the fields generated by all currents on the structure by spatially convolving the mothercell currents with the free space periodic Green's function. Besides being very costly—this procedure amounts to the time domain equivalent of attempting to sum the frequency domain Green's function directly in the spatial domain—several difficulties are encountered when discretizing the TDIE using classical MOT methods, viz. schemes that permit the iterative reconstruction of the currents one time step after another. Chief among these difficulties is the fact that the resulting MOT equations are noncausal. This difficulty however almost entirely can be circumvented by expanding the mothercell currents in a set of time-shifted basis functions that fire in a synchronized fashion with the time of arrival of the incident plane wave. The (few) remaining noncausal terms in the resulting MOT system are then eliminated by expressing ''future'' currents in terms of past ones through a

bootstrapped band-limited extrapolation procedure. These manipulations notwithstanding, the physical interpretation of the resulting MOT equations barely changes: (almost all) ''past MOT matrices'' represent fields produced by periodic current constellations active at different points in time. To avoid their costly multiplication by current expansion vectors, a new representation of these fields is called for, however. The periodic structure TDIE solver is discussed in section 2.2. The reader is encouraged to study [*Chen et al.*, 2003] as it elucidates and justifies the many parameter choices relating to the current expansion and extrapolation introduced there.

2.1.2. TDFW Expansion of Scattered Fields

[9] The proposed solver relies on a time domain Floquet wave (TDFW) representation of fields produced by periodic transient current constellations [*Capolino and Felsen*, 2003]. TDFWs are transient fields with fixed in-plane phase progression. While an infinite number of them is required to represent the fields produced by periodic current constellations for all space and time, only so-called propagating modes are required when the sources are quiescent and band limited. Within the proposed solver this fact is exploited by splitting fields produced by periodic transient current constellations into two components. First, there are the instantaneous, direct fields produced by currents in a mothercell, as well as its immediate neighbors through the action of the free space (nonperiodic) Green's function; these fields are evaluated classically for two reasons: their sources are not quiescent at their time of arrival and they act in the MOT system through matrices that are influenced by the extrapolation procedure. Second, there are the fields produced by sources that do not reside in the immediate vicinity of the mothercell: they are evaluated following their expansion in TDFWs. Because our focus here is on periodic structures that only support a finite and small number of propagating waves within their operating band, that is, structures with unit cells of linear dimensions on the order of the wavelength at the highest frequency in the incident field, TDFWs provide a very efficient means for representing these fields. The TDFW representation of fields scattered from periodic structures suitable within a TDIE-MOT context is discussed in section 2.3.

2.1.3. Blocked-FFT Acceleration of Convolutions Involving TDFW Kernels

[10] TDFWs do not constitute standard nondispersive plane waves. Indeed, their fixed transverse behavior along with their broadband character renders them dispersive in the direction perpendicular to the plane of periodicity. As a result, TDFW propagators are not time-local and costly time domain convolutions are required to track the temporal evolution of the TDFW amplitudes. Fortunately, if all sources and observation points reside in the same plane (or a finite set of distinct planes), then these convolutions can be carried out using blocked-FFT schemes [*Harrier et al.*, 1985; *Yilmaz et al.*, 2002]. This topic is discussed in section 2.4.

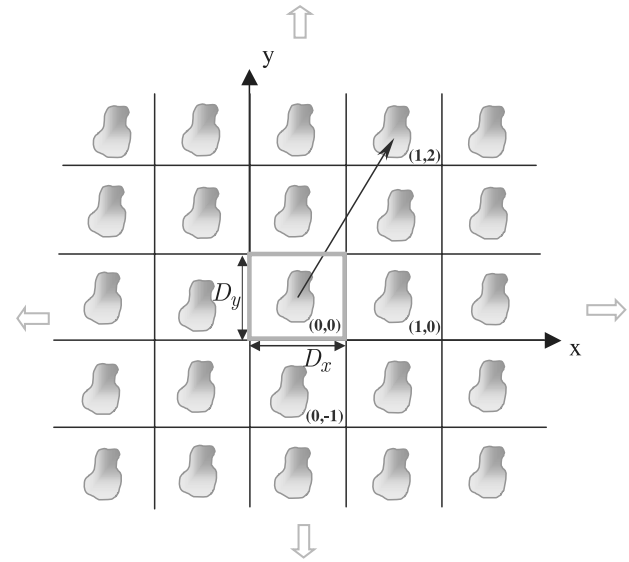

Figure 1. Top view of a doubly periodic structure comprising identical PEC elements.

2.2. Periodic Structure TDIE Solver

[11] Consider a periodic structure consisting of identical freestanding PEC elements S_{mn}, m, $n = -\infty, \infty$ residing in rectangular cells of dimensions D_x by D_y that are anchored to transverse position vectors $\boldsymbol{\rho}^c_{mn} = mD_x\,\hat{\mathbf{x}} + nD_y\,\hat{\mathbf{y}}$ and periodically arranged along x and y (Figure 1). Element S_{00} is said to reside in the mothercell. In what follows, it is assumed that the S_{mn} comprise connected or disjoint but planar patches residing in the $x - y$ plane. Later, it will be argued that the proposed scheme easily is generalized to accommodate the analysis of scattering from discretely planar periodic structures comprised planar PEC elements confined to a finite set of parallel screens; other applications of the proposed scheme are highlighted in the conclusion section. The structure is illuminated by a band-limited plane wave pulse propagating along direction $\hat{\mathbf{k}}^{inc} = -\sin\theta^{inc}\cos\phi^{inc}\hat{\mathbf{x}} - \sin\theta^{inc}\sin\phi^{inc}\hat{\mathbf{y}} - \cos\theta^{inc}\hat{\mathbf{z}}$ with electric field $\mathbf{E}^{inc}(\mathbf{r}, t, \hat{\mathbf{p}}^{inc}) = \hat{\mathbf{p}}^{inc} f(t - \hat{\mathbf{k}}^{inc} \cdot \mathbf{r}/c)$ where c and $\hat{\mathbf{p}}^{inc}$ denote the free space speed of light and the incident field's polarization, respectively. This incident field's temporal signature $f(t)$ is assumed band limited to angular frequency $\omega_{\max}$ and vanishingly small throughout the mothercell for $t < 0$. In addition, it

is assumed that both D_x and D_y are of $O(\lambda_{\min})$, where $\lambda_{\min}$ is the free space wavelength at $\omega_{\max}$. This assumption guarantees that only a fixed number of Floquet modes propagate away from the structure irrespective of the geometric features of S_{00}. Finally, to facilitate the description of the proposed FFT-accelerated field evaluator, it is assumed that the origin of the Cartesian coordinate system resides on one of the four corners of the mother cell such that $\hat{\mathbf{k}}^{inc} \cdot \boldsymbol{\rho} \leq 0$ for all $\boldsymbol{\rho} = x\hat{\mathbf{x}} + y\hat{\mathbf{y}}$ on S_{00}.

[12] Let $\mathbf{J}_{mn}(\boldsymbol{\rho}, t) = \mathbf{J}_{00}(\boldsymbol{\rho} - \boldsymbol{\rho}^c_{mn}, t - \hat{\mathbf{k}}^{inc} \cdot \boldsymbol{\rho}^c_{mn}/c)$ denote the electric current density induced on S_{mn} in response to excitation of the periodic structure by $\mathbf{E}^{inc}(\mathbf{r}, t, \hat{\mathbf{p}}^{inc})$. The current $\sum_{m,n=-\infty}^{m,n=+\infty} \mathbf{J}_{mn}(\boldsymbol{\rho}, t)$ generates the scattered field $\mathbf{E}^{sca}(\mathbf{r}, t)$. The total electric field comprises the sum of the incident and scattered fields. An electric field TDIE for $\mathbf{J}_{00}(\boldsymbol{\rho}, t)$ is constructed by forcing the temporal derivative of the total electric field tangential to S_{00} to vanish:

$$\hat{\mathbf{z}} \times \hat{\mathbf{z}} \times \frac{\partial}{\partial t}\mathbf{E}^{inc}\left(\boldsymbol{\rho}, t, \hat{\mathbf{p}}^{inc}\right) = -\hat{\mathbf{z}} \times \hat{\mathbf{z}} \times \frac{\partial}{\partial t}\mathbf{E}^{sca}(\boldsymbol{\rho}, t)\{\mathbf{J}_{00}\} \quad \boldsymbol{\rho} \in S_{00}. \tag{1}$$

The time derivative of the scattered field is expressed as

$$\begin{aligned} &-\hat{\mathbf{z}} \times \hat{\mathbf{z}} \times \frac{\partial}{\partial t}\mathbf{E}^{sca}(\boldsymbol{\rho}, t)\{\mathbf{J}_{00}\} \\ &\quad = -\frac{\mu_0}{4\pi}\frac{\partial^2}{\partial t^2}\int_{S_{00}} ds' \mathbf{J}_{00}(\boldsymbol{\rho}', t) * G(\boldsymbol{\rho}, \boldsymbol{\rho}', t) \\ &\qquad + \frac{1}{4\pi\varepsilon_0}\nabla_\rho \int_{S_{00}} ds' \left[\nabla_{\boldsymbol{\rho}'} \cdot \mathbf{J}_{00}(\boldsymbol{\rho}', t)\right] * G(\boldsymbol{\rho}, \boldsymbol{\rho}', t). \end{aligned} \tag{2}$$

In (2), $\nabla_\rho = (\partial/\partial x)\hat{\mathbf{x}} + (\partial/\partial y)\hat{\mathbf{y}}$, the Green's function is

$$G(\boldsymbol{\rho}, \boldsymbol{\rho}', t) = \sum_{m=-\infty}^{m=+\infty}\sum_{n=-\infty}^{n=+\infty} \frac{\delta\left(t - \hat{\mathbf{k}}^{inc} \cdot \boldsymbol{\rho}^c_{mn}/c - \left|\boldsymbol{\rho}' + \boldsymbol{\rho}^c_{mn} - \boldsymbol{\rho}\right|/c\right)}{\left|\boldsymbol{\rho}' + \boldsymbol{\rho}^c_{mn} - \boldsymbol{\rho}\right|}, \tag{3}$$

where the asterisk denotes temporal convolution and μ_0 and ε_0 are the free space permeability and permittivity, respectively.

[13] To solve (1) using an MOT procedure, S_{00} is approximated by triangular facets and $\mathbf{J}_{00}(\boldsymbol{\rho}, t)$ is expanded as

$$\mathbf{J}_{00}(\boldsymbol{\rho}, t) = \sum_{k=0}^{N_t}\sum_{l=1}^{N_s} I_{k,l}\mathbf{f}_l(\boldsymbol{\rho})T_{k,l}(t). \tag{4}$$

In the above equation, $I_{k,l}$ is the unknown expansion coefficient associated with space-time basis function $\mathbf{f}_l(\boldsymbol{\rho})T_{k,l}(t)$. In our implementation, the $\mathbf{f}_l(\boldsymbol{\rho})$, $l = 1, 2, \ldots, N_s$ are Rao-Wilton-Glisson functions [*Rao et al.*, 1982]; in other words, one zeroth-order divergence-conforming basis function is associated with each interior or cell boundary traversing edge in the S_{00} mesh. The number of spatial degrees of freedom, N_s, is chosen to ensure adequate spatial resolution of S_{00} and sampling of the current—lengths of edges in the discretized S_{00} should be no larger than say $\lambda_{\min}/10$. The $T_{k,l}(t)$ are time-shifted approximate prolate spheroidal wave functions (APSWFs) parameterized as $T_{k,l}(t) = P(t - t_k - t^d_l, T_p, \omega_0, \Omega)$. Here $t_k = k\Delta t$ and Δt is the time step size; the latter, and consequently N_t, are chosen such that representation (4) oversamples (from the Nyquist rate) all temporal waveforms by a factor between 5 and 10. The basis function dependent time shift imposed on the lth spatial basis function is $t^d_l = \hat{\mathbf{k}}^{inc} \cdot \boldsymbol{\rho}^c_l/c$ where $\boldsymbol{\rho}^c_l$ is the center of the edge defining $\mathbf{f}_l(\boldsymbol{\rho})$; these shifts are introduced to mitigate the appearance of noncausal terms appearing in the MOT equations that result upon discretizing (2) when the structure under analysis is obliquely excited (the procedure can be thought of as the time domain equivalent of frequency domain phase extraction schemes and also is used when testing the discretized integral equation—see below and *Chen et al.* [2003]). The APSWFs, originally proposed by *Knab* [1979], are

$$P\left(t, T_p, \omega_0, \Omega\right) = \frac{\omega_0}{\pi}\frac{\operatorname{sinc}(\omega_0 t)}{\sinh\left(\Omega T_p\right)}\frac{\sin\left(\Omega T_p\sqrt{\left(\frac{t}{T_p}\right)^2 - 1}\right)}{\sqrt{\left(\frac{t}{T_p}\right)^2 - 1}}, \tag{5}$$

where $\omega_0 = 0.5(\omega_s + \omega_{\max})$, $\Omega = 0.5(\omega_s - \omega_{\max})$, $\omega_s = \pi/\Delta t > \omega_{\max}$, and $T_p = N_{pro}\Delta t$. The APSWFs are used as the temporal basis functions because of their interpolatory properties: they are strictly band limited to ω_s and virtually time limited as they become vanishingly small for $|t| > (N_{pro} + \frac{1}{2})\Delta t$ for large enough time bandwidth products ΩT_p. As a result, each temporal basis function only covers $(2N_{pro} + 1)$ time steps; typically, to ensure accuracies in line with those associated with the above discussed spatial representations, N_{pro} is chosen between 3 and 5 (this and other parameters along with their typical values are collected in Table 1).

[14] Substituting (4) into (2) and testing the resulting equation using each of the $\mathbf{f}_l(\boldsymbol{\rho})$, $l = 1, 2, \ldots, N_s$, at time $t_i + t^d_l$, $i = 1, \ldots, N_t$, results in the following matrix equation:

$$\sum_{k=-N_{adv}}^{0} \mathbf{Z}_k\mathbf{I}_{i-k} = \mathbf{V}_i - \sum_{k=1}^{i-1} \mathbf{Z}_k\mathbf{I}_{i-k}. \tag{6}$$

Table 1. Description of the Parameters in the Paper

Parameter	Function	Typical Value
N_s	Number of spatial degrees of freedom	
N_t	Number of temporal degrees of freedom	
N_{pro}	APSWF half width in time steps	3–5
N_{adv}	Number of advanced currents in noncausal MOT system (6)	0–3
N_{ext}	Number of past current coefficients used to extrapolate advanced ones to convert noncausal MOT system (6) to causal MOT system (10)	3–5
N_{del}	Number of past current coefficients whose field is evaluated classically, without relying on TDFW decomposition	5–7
N_{exc}	Maximum length of all spatial basis functions in time steps measured by the incident field	1–2
N_{p2}	Half width of the modified APSWFs in time steps	5–8
ξ^*	One of the two parameters to determine N_{mod}, the number of "propagating modes"	1.1–1.3
ϑ	One of the two parameters to determine N_{mod}, the number of "propagating modes"	1–4

Here N_{adv} denotes the number of future/advanced current vectors that appear in the MOT system because of the structure's periodicity and use of the APSWFs; it was shown by *Chen et al.* [2003] that N_{adv} is independent of the mothercell dimensions (in practice, N_{adv} always is less than 3). The $\mathbf{I}_i$ and $\mathbf{V}_i$ are vectors of length N_s, $[\mathbf{I}_i]_l = I_{i,l}$, $i = 1, \ldots, N_t$,

$$[\mathbf{V}_i]_l = -\int_{S_{00}} ds\ \mathbf{f}_l(\rho) \cdot \left[\frac{\partial}{\partial t}\mathbf{E}^{inc}\left(\boldsymbol{\rho}, t, \hat{\mathbf{p}}^{inc}\right)\right]_{t=t_i+t_l^d}, \quad (7)$$

and $\mathbf{Z}_k$, $k = -N_{adv}, -N_{adv}+1, \ldots, 0, \ldots, N_t - 1$ are matrices of dimensions $N_s \times N_s$ with elements

$$[\mathbf{Z}_k]_{ll'} = \Big[-\frac{\mu_0}{4\pi}\frac{\partial^2}{\partial t^2}\int_{S_{00}} ds\ \mathbf{f}_l(\boldsymbol{\rho}) \cdot \int_{S_{00}} ds'\ \mathbf{f}_{l'}(\boldsymbol{\rho}') T_{0,l'}(t) * G(\boldsymbol{\rho}, \boldsymbol{\rho}', t) - \frac{1}{4\pi\varepsilon_0}\int_{S_{00}} ds\left[\nabla_\rho \cdot \mathbf{f}_l(\boldsymbol{\rho})\right] \cdot \int_{S_{00}} ds'\left[\nabla_{\boldsymbol{\rho}'} \cdot \mathbf{f}_{l'}(\boldsymbol{\rho}')\right] T_{0,l'}(t) * G(\boldsymbol{\rho}, \boldsymbol{\rho}', t)\Big]_{t=t_k+t_l^d}. \quad (8)$$

Equation (6) cannot be solved by a standard MOT procedure because at time step i future coefficients are involved. This difficulty is resolved by extrapolating these future coefficients through a band-limited extrapolator [see *Chen et al.*, 2003]. In essence, the future current vectors (approximately) can be expressed in terms of present and past current vectors as

$$\mathbf{I}_{i-k} = \sum_{q=0}^{N_{ext}} A_q^k \mathbf{I}_{i-q} \quad \forall\ k = -N_{adv}, \ldots, -1, \quad (9)$$

where N_{ext} denotes the number of past current samples used in the extrapolation and the A_q^k are extrapolation coefficients for the kth future current vector associated with the qth past current vector (all relative to the present time step, i); these coefficients can be obtained using the prolate-based extrapolation scheme detailed by *Cadzow* [1979] and *Slepian and Pollak* [1961]. Upon inserting (9) into (6), the latter is recast as

$$\tilde{\mathbf{Z}}_0 \mathbf{I}_i = \mathbf{V}_i - \sum_{k=1}^{i-1} \tilde{\mathbf{Z}}_k \mathbf{I}_{i-k}, \quad (10)$$

with $\tilde{\mathbf{Z}}_q = \mathbf{Z}_q + \sum_{k=-N_{adv}}^{-1} A_q^k \mathbf{Z}_k$ for $q = 0, \ldots, N_{ext}$, and $\tilde{\mathbf{Z}}_q = \mathbf{Z}_q$ for $q > N_{ext}$. Often, just like N_{pro}, N_{ext} is chosen in between 3 and 5 [*Chen et al.*, 2003]. In what follows, however, it is assumed that $N_{ext} < N_{pro}$, which implies that matrices $\tilde{\mathbf{Z}}_q$ for $q > N_{pro}$ are unaffected by the extrapolation. In other words, past space-time basis functions that are quiescent at time i enter the MOT system through matrices $\tilde{\mathbf{Z}}_i = \mathbf{Z}_i$ that describe fields produced by periodic constellations of past currents. This fact will prove to be important in the construction of a TDFW-based scheme. Equation (10) can be solved by a standard MOT procedure to obtain current vectors for all time steps. Since $\tilde{\mathbf{Z}}_0$ is not diagonal, a nonstationary iterative solver such as (TF)QMR [*Saad*, 1996] is used.

[15] The dominant computational cost in the above scheme arises from the need to repeatedly evaluate the right-hand side (RHS) of (10) for all time steps and scales as $O(N_s^2 N_t^3)$. Indeed, the RHS of (10) is a measure of the field at N_s observers on S_{00}, produced by all sources in the mothercell plus those in surrounding cells whose field at a given time step has reached the mothercell. Obviously, the number of such sources grows larger with time step and N_t; it is easily shown that, at a given time step in the analysis, there are on average a total of $O(N_s N_t^2)$ of them. Evaluating their field at $O(N_s)$ observers in the mothercell thus costs $O(N_s^2 N_t^2)$ CPU resources for one time step, and $O(N_s^2 N_t^3)$ for all time steps.

2.3. TDFW Scheme

[16] This subsection details a TDFW-based scheme to rapidly evaluate the sum on the RHS of (10). The scheme hinges on an expansion of the periodic time domain

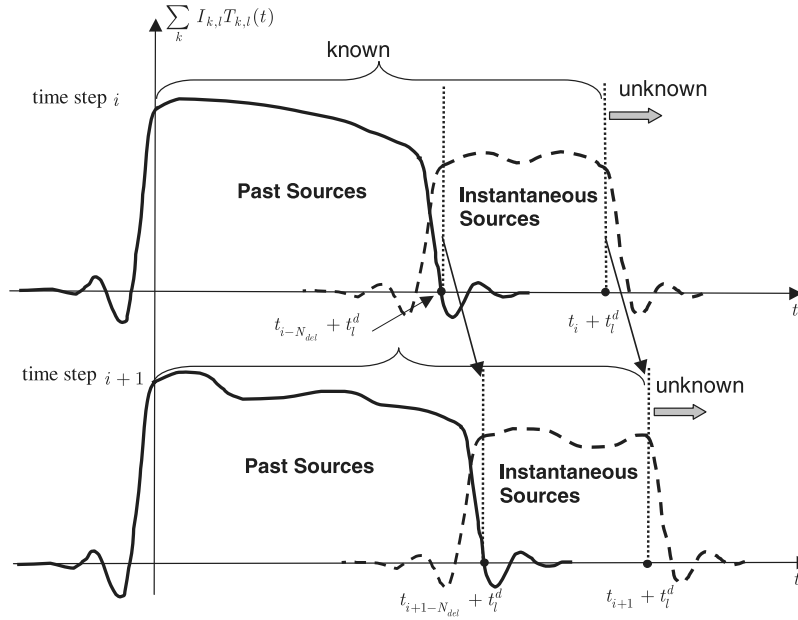

Figure 2. Illustration of the split of the source time signature in the TDFW scheme.

Green's function in TDFWs [*Capolino and Felsen*, 2002, 2003; *Felsen and Capolino*, 2000]. As TDFWs represent efficiently only fields produced by quiescent band-limited sources—see below—the time signature of the source $\mathbf{J}_{00}(\boldsymbol{\rho}, t)$ (available at time step i) is decomposed as (Figure 2)

$$\sum_{l=1}^{N_s} \mathbf{f}_l(\boldsymbol{\rho}) \sum_{k=i-N_{del}+1}^{i-1} I_{k,l}T_{k,l}(t) + \sum_{l=1}^{N_s} \mathbf{f}_l(\boldsymbol{\rho}) \sum_{k=1}^{i-N_{del}} I_{k,l}T_{k,l}(t). \tag{11}$$

At time step i, the known signature, that is, the values prior to time step i, is decomposed into two components, instantaneous sources (dashed line in Figure 2, the first term of (11)) and past sources (solid line in Figure 2, the second term in (11)), in temporal dimension according to the delay index N_{del}. Note the width of the instantaneous sources is fixed from time step i to time step $i + 1$. Meanwhile, the width of the past sources is increased by a time step size. The parameter N_{del} in (11) is chosen to satisfy $N_{del} > N_{pro} + N_{exc}$, with N_{exc} a small integer defined as

$$N_{exc} = \max_{1\le l\le N_s} \left\lceil \frac{\left|\hat{\mathbf{k}}^{inc} \cdot \left(\boldsymbol{\rho}_l^c - \boldsymbol{\rho}_l^{any}\right)\right|}{c\Delta t} \right\rceil, \tag{12}$$

where $\lceil\cdot\rceil$ selects the smallest integer larger than the argument and $\boldsymbol{\rho}_l^{any}$ denotes an arbitrary point in the support of $\mathbf{f}_l(\boldsymbol{\rho})$. Note that N_{pro} is the half width of the temporal basis functions $T_{k,l}(t)$, and N_{exc} measures the maximum size of all the Rao-Wilton-Glisson functions with respect to the incident angle. As a result, the choice of $N_{del} > N_{pro} + N_{exc}$ guarantees that the past sources are in essence quiescent at time step i for all the possible observers. Because $N_{ext} < N_{pro} < N_{del}$, it also implies that all past sources enter the MOT update equations through the original matrices $\boldsymbol{Z}_i$, unaffected by the extrapolation procedure. In other words, evaluation of the contribution of the past sources to the RHS of (10) requires the computation of the fields they produced, and nothing more. Note that the choice of $T_{k,l}(t)$ guarantees that both the instantaneous and past sources are band limited in time. It is noted that N_{del} is a constant of $O(1)$ that, just like N_{pro}, N_{adv}, and N_{ext}, does not depend on N_s or N_t. The reason for the presence of the term N_{exc} in the above inequality for N_{del} is subtle and will become clear when discussing the aforementioned blocked FFT accelerator (section 2.4).

[17] The above definition of instantaneous and past sources prompts a similar decomposition of the sum on the RHS of (10) as

$$\sum_{k=1}^{i-1} \tilde{\mathbf{Z}}_k \mathbf{I}_{i-k} = \sum_{k=1}^{N_{del}-1} \tilde{\mathbf{Z}}_k \mathbf{I}_{i-k} + \sum_{k=N_{del}}^{i-1} \tilde{\mathbf{Z}}_k \mathbf{I}_{i-k}. \tag{13}$$

The first and second terms on the RHS of (13) define the instantaneous and delayed fields at time step i, respectively. Instantaneous fields, viz. fields produced by instantaneous currents, can be computed classically, through multiplication of the sparse matrices $\tilde{\mathbf{Z}}_k$, $k = 1,\ldots, N_{del} - 1$ with the current vectors $\mathbf{I}_{i-k}$, $k = 1,\ldots, N_{del} - 1$. Because N_{del} is of $O(1)$ and the linear cell dimensions are of $O(\lambda_{\min})$, this operation requires $O(N_s^2)$ operations per time step and thus no more than $O(N_s^2 N_t)$ for the entire simulation. Delayed fields, instead, are computed by casting them in terms of TDFWs. To elucidate the introduction of TDFWs into the MOT framework, consider the following expressions for $\left[\sum_{k=N_{del}}^{i-1} \mathbf{Z}_k \mathbf{I}_{i-k}\right]_l$, viz. the lth component of the delayed field vector at time step i:

$$\begin{aligned}\left[\sum_{k=N_{del}}^{i-1} \mathbf{Z}_k \mathbf{I}_{i-k}\right]_l = \sum_{l'=1}^{N_s}\Bigg[& -\frac{\mu_0}{4\pi}\frac{\partial^2}{\partial t^2}\int_{S_{00}} ds\, \mathbf{f}_l(\boldsymbol{\rho}) \\ & \cdot \int_{S_{00}} ds' \mathbf{f}_{l'}(\boldsymbol{\rho}') \sum_{k=1}^{i-N_{del}} I_{k,l'} T_{k,l'}(t) \\ & * G(\boldsymbol{\rho}, \boldsymbol{\rho}', t) - \frac{1}{4\pi\varepsilon_0}\int_{S_{00}} ds \left[\nabla_{\boldsymbol{\rho}} \cdot \mathbf{f}_l(\boldsymbol{\rho})\right] \\ & \cdot \int_{S_{00}} ds' \cdot \left[\nabla_{\boldsymbol{\rho}'} \cdot \mathbf{f}_{l'}(\boldsymbol{\rho}')\right] \sum_{k=1}^{i-N_{del}} I_{k,l'} T_{k,l'}(t) \\ & * G(\boldsymbol{\rho}, \boldsymbol{\rho}', t)\Big]_{t=t_i+t_l^d}. \end{aligned} \tag{14}$$

This equation follows directly from (8). Note that none of the integrands in (14) possess spatial singularities because they model couplings with (integer) delays greater than N_{del} or equivalently, between spatially separated sources and observers.

[18] *Capolino and Felsen* [2003] show that the periodic time domain Green's function can be expanded in TDFWs as

$$\begin{aligned} G(\boldsymbol{\rho}, \boldsymbol{\rho}', t) &= \sum_{p=-\infty}^{\infty}\sum_{q=-\infty}^{\infty} A_{pq}^{FW}(\boldsymbol{\rho}, \boldsymbol{\rho}', t) \\ &= \sum_{p=0}^{\infty}\sum_{q=-\infty}^{\infty} \beta_{pq} \Re e\left[A_{pq}^{FW}(\boldsymbol{\rho}, \boldsymbol{\rho}', t)\right], \end{aligned} \tag{15}$$

where $\beta_{pq} = 1$ for $p = 0$ and $\beta_{pq} = 2$ for $p \neq 0$, $\Re e[\cdot]$ selects the real part of its argument,

$$A_{pq}^{FW}(\boldsymbol{\rho}, \boldsymbol{\rho}', t) = \frac{c e^{-j\boldsymbol{\alpha}_{pq}\cdot(\boldsymbol{\rho}, -\boldsymbol{\rho}')}}{2D_x D_y\sqrt{1-\eta^2}} e^{j\tilde{\omega}_{pq}\tau} J_0\left[\tilde{\omega}_{pq}\tau\right] U(\tau), \tag{16}$$

$j = \sqrt{-1}$, $J_0(\cdot)$ denotes the zeroth-order Bessel function, $U(\cdot)$ is the Heaviside step function,

$$\begin{aligned} &\eta = \sin\theta^{inc} \\ &\boldsymbol{\alpha}_{pq} = 2\pi p/D_x \hat{\mathbf{x}} + 2\pi q/D_y \hat{\mathbf{y}} \\ &\boldsymbol{\alpha}_{pq}^2 = (2\pi p/D_x)^2 + (2\pi q/D_y)^2 \\ &\hat{\mathbf{u}}_1 = \cos\phi^{inc}\hat{\mathbf{x}} + \sin\phi^{inc}\hat{\mathbf{y}} \\ &\bar{\omega}_{pq} = \tfrac{\eta c}{1-\eta^2}\hat{\mathbf{u}}_1 \cdot \boldsymbol{\alpha}_{pq} \\ &\tilde{\omega}_{pq} = \sqrt{\bar{\omega}_{pq}^2 + \boldsymbol{\alpha}_{pq}^2 c^2/(1-\eta^2)} \\ &\tau = t - t_0, \end{aligned} \tag{17}$$

and $t_0 = \eta\, \hat{\mathbf{u}}_1 \cdot (\boldsymbol{\rho} - \boldsymbol{\rho}')/c$. The second equality in (15) is due to the fact that $A_{pq}^{FW}(\boldsymbol{\rho}, \boldsymbol{\rho}', t)$ and $A_{(-p)(-q)}^{FW}(\boldsymbol{\rho}, \boldsymbol{\rho}', t)$ are complex conjugates of one another. Before using the above TDFW expansion of the Green's function in (14), two important observations are in order. First, although the summation in (15) comprises an infinite number of terms, upon convolution of the Green's function with the band-limited and essentially time-limited APSWF, only so-called propagating modes should be retained provided that the field is observed no earlier than $t_0 + \vartheta\Delta t$ seconds after the APSWF (essentially) vanishes with $\vartheta > 1$ a dimensionless parameter. The propagating modes are those with modal indices satisfying $\min(|\tilde{\omega}_{pq} + \bar{\omega}_{pq}|, |\tilde{\omega}_{pq} - \bar{\omega}_{pq}|)/\omega_s < \xi^*$, – recall that ω_s is the bandwidth of the APSWF, with $\xi^* > 1$ another dimensionless parameter. In other words, the convolution of the APSWF with the nonpropagating modes essentially vanishes for times t starting $t_0 + \vartheta\Delta t$ seconds after the APSWF elapses. This observation is demonstrated in Appendix A, which demonstrates the fast convergence of the truncated TDFW series with increasing ϑ and ξ^*; typical values of ϑ and ξ^* in line with accuracies of spatial current expansions are 3 and 1.2, respectively. It is also shown in Appendix A that the total number of propagating TDFWs retained in the expansion, denoted as N_{mod}, is proportional to the area of the mothercell. Because the linear cell dimensions are of $O(\lambda_{\min})$, N_{mod} is of $O(1)$, that is, independent of N_s and N_t. Second, the Floquet wave in (16) can be expressed as

$$\begin{aligned} A_{pq}^{FW}(\boldsymbol{\rho}, \boldsymbol{\rho}', t) = & e^{-j\boldsymbol{\alpha}_{pq}\cdot\boldsymbol{\rho}}\delta[t - \eta\hat{\mathbf{u}}_1\cdot\boldsymbol{\rho}/c] \\ & * A_{pq}^{FW}(\mathbf{0}, \mathbf{0}, t) \\ & * e^{j\boldsymbol{\alpha}_{pq}\cdot\boldsymbol{\rho}'}\delta[t + \eta\hat{\mathbf{u}}_1\cdot\boldsymbol{\rho}'/c]. \end{aligned} \tag{18}$$

Artificial as this decomposition might seem at present, it has important computational consequences as demonstrated next.

[19] Indeed, use of (15)–(18) and the realization that only propagating modes are needed in the TDFW ex-

pansion of the Green's operator for the signals considered in (14) yields the following expression for the delayed fields at time step i produced by all past sources and tested by $\mathbf{f}_l(\boldsymbol{\rho})$, $l = 1,\ldots, N_s$:

$$\begin{aligned}
&\left[\sum_{k=N_{del}}^{i-1}\mathbf{Z}_k\mathbf{I}_{i-k}\right]_l \\
&\quad=-\frac{\mu_0}{4\pi}\sum_{\{(p,q)\text{ is propagating mode}\}}\beta_{pq} \\
&\qquad\cdot\Re e\left\{\int_{S_{00}}ds\,\mathbf{f}_l(\boldsymbol{\rho})\cdot e^{-j\boldsymbol{\alpha}_{pq}\cdot\boldsymbol{\rho}}\delta\left[t-\frac{\eta\hat{\mathbf{u}}_1\cdot\boldsymbol{\rho}}{c}\right]\right. \\
&\qquad* A_{pq}^{FW}(\mathbf{0},\mathbf{0},t) \\
&\qquad* \sum_{l'=1}^{N_s}\int_{S_{00}}ds' e^{j\boldsymbol{\alpha}_{pq}\cdot\boldsymbol{\rho}'}\delta\left[t+\frac{\eta\hat{\mathbf{u}}_1\cdot\boldsymbol{\rho}'}{c}\right] \\
&\qquad\left.* \sum_{k=1}^{i-N_{del}}\mathbf{f}_{l'}(\boldsymbol{\rho}')I_{k,l'}\frac{d^2}{dt^2}T_{k,l'}(t)\right\}_{t=t_i+t_l^d} \\
&\qquad-\frac{1}{4\pi\varepsilon_0}\sum_{\{(p,q)\text{ is propagating mode}\}}\beta_{pq} \\
&\qquad\cdot\Re e\left\{\int_{S_{00}}ds\left[\nabla_{\boldsymbol{\rho}}\cdot\mathbf{f}_l(\boldsymbol{\rho})\right]e^{-j\boldsymbol{\alpha}_{pq}\cdot\boldsymbol{\rho}}\delta\left[t-\frac{\eta\hat{\mathbf{u}}_1\cdot\boldsymbol{\rho}}{c}\right]\right. \\
&\qquad* A_{pq}^{FW}(\mathbf{0},\mathbf{0},t) \\
&\qquad* \sum_{l'=1}^{N_s}\int_{S_{00}}ds' e^{j\boldsymbol{\alpha}_{pq}\cdot\boldsymbol{\rho}'}\delta\left[t+\frac{\eta\hat{\mathbf{u}}_1\cdot\boldsymbol{\rho}'}{c}\right] \\
&\qquad\left.* \sum_{k=1}^{i-N_{del}}\left[\nabla_{\boldsymbol{\rho}'}\cdot\mathbf{f}_{l'}(\boldsymbol{\rho}')\right]I_{k,l'}T_{k,l'}(t)\right\}_{t=t_i+t_l^d}.
\end{aligned}\tag{19}$$

This equation is the crux of the proposed TDFW scheme for evaluating delayed fields produced by past sources and its interpretation within a computational framework is elucidated next. First, note that the first and second terms on the RHS of (19) describe vector and scalar potential contributions to the delayed field, respectively. The evaluation of each term in (19) comprises three temporal convolutions. As for the vector potential term, these three convolutions are $\sum_{l'=1}^{N_s}\int_{S_{00}}ds' e^{j\boldsymbol{\alpha}_{pq}\cdot\boldsymbol{\rho}'}\delta\left[t+\frac{\eta\hat{\mathbf{u}}_1\cdot\boldsymbol{\rho}'}{c}\right]$ * $\sum_{k=1}^{i-N_{del}}\mathbf{f}_{l'}(\boldsymbol{\rho}')I_{k,l'}\frac{d}{dt^2}T_{k,l'}(t)$ (convolution 1), $A_{pq}^{FW}(\mathbf{0},\mathbf{0},t)$ * (convolution 2), and $\int_{S_{00}}ds\;\mathbf{f}_l(\boldsymbol{\rho})e^{-j\boldsymbol{\alpha}_{pq}\cdot\boldsymbol{\rho}}\;\delta\left[t-\frac{\eta\hat{\mathbf{u}}_1\cdot\boldsymbol{\rho}}{c}\right]$ * (convolution 3), where the asterisk indicates temporal convolution. The three convolutions for the scalar potential term can be similarly identified. These convolutions are carried out on a time step by time step basis, resulting in the three-stage scheme for evaluating $\left[\sum_{k=N_{del}}^{i-1}\mathbf{Z}_k\mathbf{I}_{i-k}\right]_l$ described next.

[20] 1. Project the sources temporal signatures onto "source rays" (Figure 3a). Vector and scalar source rays $\mathbf{S}_{pq,i}^A(t)$ and $S_{pq,i}^{\Phi}(t)$ for TDFW mode (p, q) and time step i are defined as

$$\begin{aligned}
\mathbf{S}_{pq,i}^A(t)&=\sum_{l'=1}^{N_s}\int_{S_{00}}ds' e^{j\boldsymbol{\alpha}_{pq}\cdot\boldsymbol{\rho}'}\delta\left[t+\frac{\eta\hat{\mathbf{u}}_1\cdot\boldsymbol{\rho}'}{c}\right] \\
&\quad* \mathbf{f}_{l'}(\boldsymbol{\rho}')I_{i-N_{del},l'}\frac{d^2}{dt^2}T_{i-N_{del},l'}(t) \\
S_{pq,i}^{\Phi}(t)&=\sum_{l'=1}^{N_s}\int_{S_{00}}ds' e^{j\boldsymbol{\alpha}_{pq}\cdot\boldsymbol{\rho}'}\delta\left[t+\frac{\eta\hat{\mathbf{u}}_1\cdot\boldsymbol{\rho}'}{c}\right] \\
&\quad* \left[\nabla_{\boldsymbol{\rho}'}\cdot\mathbf{f}_{l'}(\boldsymbol{\rho}')\right]I_{i-N_{del},l'}T_{i-N_{del},l'}(t).
\end{aligned}\tag{20}$$

Vector and scalar source rays $\mathbf{S}_{pq}^A(t)$ and $S_{pq}^{\Phi}(t)$ for TDFW mode (p, q) are defined as $\mathbf{S}_{pq}^A(t)=\sum_i\mathbf{S}_{pq,i}^A(t)$ and $S_{pq}^{\Phi}(t)=\sum_i S_{pq,i}^{\Phi}(t)$, respectively. As seen from (20), vector and scalar source rays are constructed by carrying out convolution 1 in (19) between source signals residing at spatial locations $\boldsymbol{\rho}'$ and delay operators $\delta[t+\eta\,\hat{\mathbf{u}}_1\cdot\boldsymbol{\rho}'/c]$. In Figure 3a, the cross section of the mother cell S_{00} is shown for illustration. The top plots of Figure 3a depict the time signatures of the scalar source signals at points $\boldsymbol{\rho}_{l'_1}^c$ and $\boldsymbol{\rho}_{l'_2}^c$ at time step i. The bottom plot of Figure 3a shows the formation of source ray $S_{pq,i}^{\Phi}(t)$ via projecting all the scalar sources onto the point $\mathbf{O}=(x=0, y=0, z=0)$ along the direction of $\hat{\mathbf{k}}^{inc}$. Note that the scalar source ray $S_{pq,i}^{\Phi}(t)$ is a complex quantity, although it is drawn as a real-valued function in Figure 3a.

[21] 2. Construct "field rays" (Figure 3b). Vector and scalar field rays $\mathbf{F}_{pq,i}^A(t)$ and $F_{pq,i}^{\Phi}(t)$ for TDFW mode (p, q) and time step i are defined as

$$\begin{aligned}
\mathbf{F}_{pq,i}^A(t)&=A_{pq}^{FW}(\mathbf{0},\mathbf{0},t)*\mathbf{S}_{pq,i}^A(t) \\
F_{pq,i}^{\Phi}(t)&=A_{pq}^{FW}(\mathbf{0},\mathbf{0},t)*S_{pq,i}^{\Phi}(t).
\end{aligned}\tag{21}$$

Vector and scalar field rays $\mathbf{F}_{pq}^A(t)$ and $F_{pq}^{\Phi}(t)$ for TDFW mode (p, q) are defined as

$$\begin{aligned}
\mathbf{F}_{pq}^A(t)&=\sum_{i=1}^{\lfloor t/\Delta t\rfloor}\mathbf{F}_{pq,i}^A(t) \\
F_{pq}^{\Phi}(t)&=\sum_{i=1}^{\lfloor t/\Delta t\rfloor}F_{pq,i}^{\Phi}(t),
\end{aligned}\tag{22}$$

where $\lfloor\cdot\rfloor$ selects the largest integer smaller than the argument. Field rays represent the time signature of the TDFW-decomposed delayed field observed at the spatial origin. In (22), the upper limit in the summation over i is $\lfloor t/\Delta t\rfloor$, because $\mathbf{S}_{pq,\lfloor t/\Delta t\rfloor}^A(t)/S_{pq,\lfloor t/\Delta t\rfloor}^{\Phi}(t)$ is the last available vector/scalar source ray at time t.

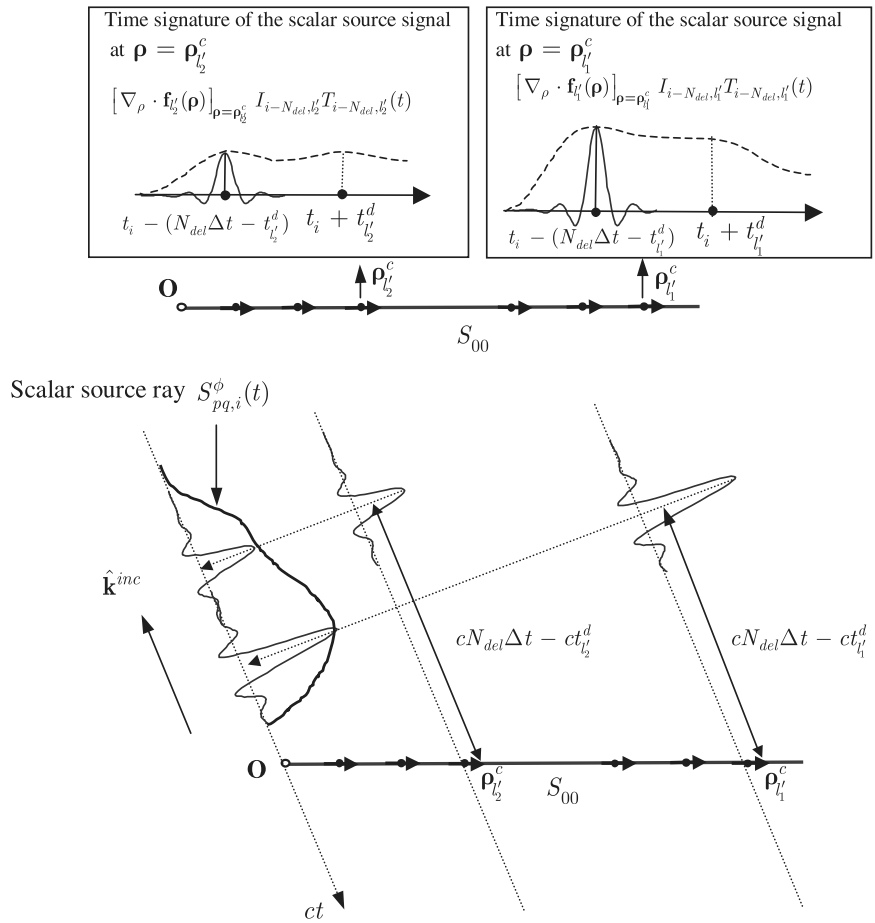

Figure 3a. Pictorial description of the first stage in a three-stage scheme.

[22] 3. Project the "field rays" onto the observers (Figure 3c):

$$\left[\sum_{k=N_{del}}^{i-1} \mathbf{Z}_k \mathbf{I}_{i-k}\right]_l = -\frac{\mu_0}{4\pi} \sum_{\{(p,q)\text{ is propagating mode}\}} \beta_{pq} \cdot \Re e\left\{ \int_{S_{00}} ds \mathbf{f}_l(\boldsymbol{\rho}) \cdot e^{-j\boldsymbol{\alpha}_{pq}\cdot\boldsymbol{\rho}} \delta\left[t - \frac{\eta\hat{\mathbf{u}}_1 \cdot \boldsymbol{\rho}}{c}\right] * \mathbf{F}^A_{pq}(t) \right\}_{t=t_i+t^d_l} - \frac{1}{4\pi\varepsilon_0} \cdot \sum_{\{(p,q)\text{ is propagating mode}\}} \beta_{pq} \cdot \Re e\left\{ \int_{S_{00}} ds \left[\nabla_\rho \cdot \mathbf{f}_l(\boldsymbol{\rho})\right] e^{-j\boldsymbol{\alpha}_{pq}\cdot\boldsymbol{\rho}} \cdot \delta\left[t - \frac{\eta\hat{\mathbf{u}}_1 \cdot \boldsymbol{\rho}}{c}\right] * F^\phi_{pq}(t) \right\}_{t=t_i+t^d_l}. \quad (23)$$

In Figure 3c, the time signatures of the scalar field ray $F^\phi_{pq}(t)$ observed at the points $\boldsymbol{\rho}^c_{l_1}$ and $\boldsymbol{\rho}^c_{l_2}$ are shown in the upper right and left insets, respectively. These time signatures are obtained by projecting the scalar field rays observed at point **O** onto the observation points along the direction of $\hat{\mathbf{k}}^{inc}$.

[23] Next, the computational implications and complexity of the above three-stage decomposition and scheme are elucidated. Before doing so, however, it is useful to call attention to similarities between the proposed method and the plane wave time domain algorithm [*Ergin et al.*, 1998] or fast multipole methods in general. Indeed, like the latter, the proposed field evaluator realizes computational savings by not having each source and observer communicate directly with one another; instead, they connect through a set of uncoupled though common carriers, TDFWs in the present scheme. Information contained in the delayed fields produced by the $O(N_s)$ sources is compressed/aggregated (step 1) into a data stream of N_{mod} TDFWs, before being propagated (step 2) and uncompressed/disaggregated

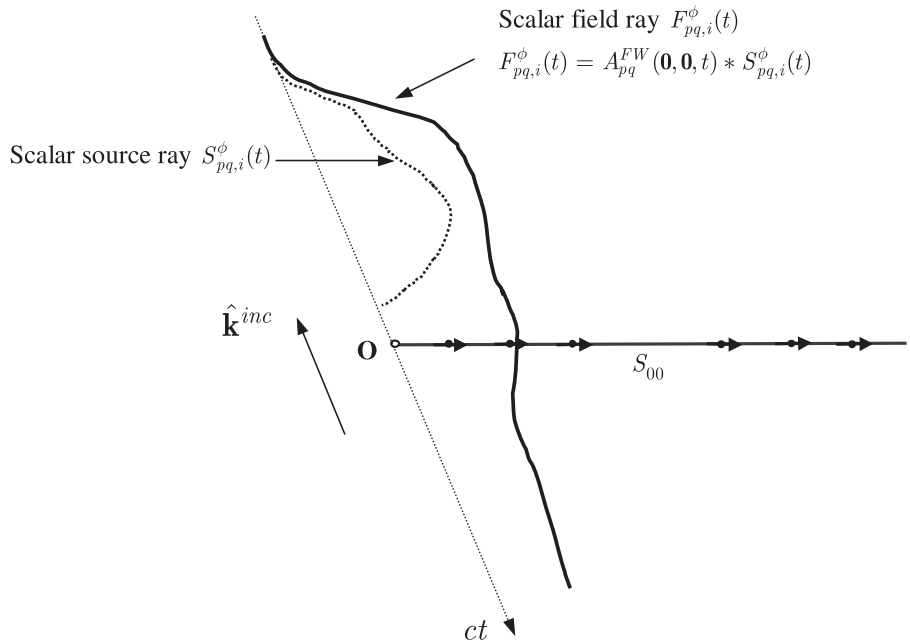

Figure 3b. Pictorial description of the second stage in a three-stage scheme. The scalar field ray $F^{\phi}_{pq,i}(t)$ is formed via convolving the scalar source ray $S^{\phi}_{pq,i}(t)$ with the TDFW operator $A^{FW}_{pq}(\mathbf{0}, \mathbf{0}, t)$.

(step 3) to obtain $O(N_s)$ observer fields. In view of the properties of the temporal basis functions used — recall that they are in essence time limited — all projections inherent in steps 1 and 3 are strictly local and therefore the computational costs of (a single of) these steps scales linearly in N_s and N_{mod} and is independent of N_t; because steps 1 and 3 are carried out for all N_t time steps, their total cost for the duration of the analysis thus scales as $O(N_{\text{mod}}N_tN_s)$. The cost of step 2 scales linearly in N_{mod} and is independent of N_s. Because step 2 requires a costly temporal convolution of source rays with the nonlocal temporal propagator $A^{FW}_{pq}(\mathbf{0}, \mathbf{0}, t)$, its cost scales as $O(N_{\text{mod}}N_t^2)$ if the convolution is evaluated classically. Fortunately, the propagator $A^{FW}_{pq}(\mathbf{0}, \mathbf{0}, t)$ is invariant with respect to temporal shifts, thereby allowing the above convolutions to be evaluated using blocked FFTs, as described in the next paragraph, at a cost of $O(N_t \log^2 N_t)$; the computational cost of executing step 2 for all time steps thus scales as $O(N_{\text{mod}} N_t \log^2 N_t)$. The total cost of the proposed scheme therefore scales as $O(N_s^2N_t + N_sN_{\text{mod}}N_t + N_{\text{mod}}N_t \log^2 N_t)$ with the first, second, and third terms in this estimate stemming from the evaluation of the instantaneous fields, steps 1 and 3, and step 2 of the delayed field evaluation, respectively. Because the above assumptions guarantee that N_{mod} is of $O(1)$, the scheme's cost essentially would scale linearly in both N_s and N_t, were it not for the cost of evaluating instantaneous fields. Fortunately, if N_s becomes large—this means under the current assumptions that the mothercell would be packed with many spatial unknowns to resolve fine geometric features of the scatterer (an unlikely scenario)—then this cost can be reduced to $O(N_sN_t \log^2 N_t)$ by using a low-frequency plane wave time domain algorithm [*Aygün et al.*, 2000] or time domain adaptive integral method [*Yilmaz et al.*, 2003]. This last option was not exercised in our current implementation, as our focus was on relatively simple mothercells. Also, note that the case of an electromagnetically large unit mothercell, viz. one supporting many propagating modes that in number might scale as N_s, remains problematic. Although even in this scenario the proposed solver outperforms the classical solvers *Chen et al.* [2003], it remains prohibitively expensive. The situation is no different for frequency domain integral equation-based schemes for analyzing scattering from periodic structures: to the authors' knowledge, at present, no fast solver for such structures exists if the number of unknowns grows proportionally with the number of propagating modes. The usefulness of such a solver is, however, even more questionable as that of one capable of analyzing highly resolved mothercells.

2.4. Blocked FFT-Based Evaluation of the Temporal Convolutions

[24] To describe a cost-effective FFT-based scheme for evaluating temporal convolutions requisite in step 2 of the

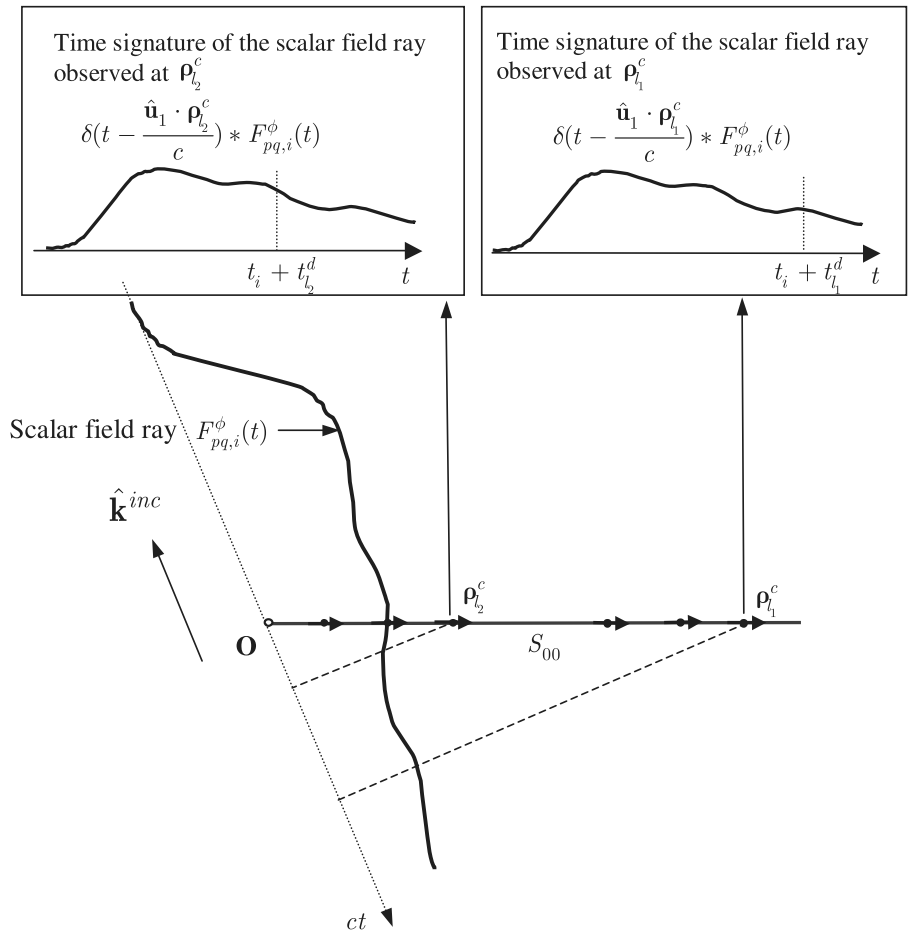

Figure 3c. Pictorial description of the third stage in a three-stage scheme.

above scheme, a discussion of the spectral properties and representation of source and field rays is in order. Equation (4) expands currents in terms of essentially time-limited APSWFs of bandwidth $\omega_s > \omega_{\max}$. These APSWFs permit the discrete representation/interpolation of the current with exponential accuracy. Equation (14) casts source rays in terms of scaled and shifted such APSWFs. It follows that the discrete representation/exponentially accurate local interpolation and manipulation of source rays requires the introduction of an even more resolved interpolant, itself capable of representing the original APSWFs used to expand the current. To this end, source rays are sampled at time intervals $\Delta t/2$ and represented in terms of a new set of modified APSWFs $P(t, \tilde{T}_p, \tilde{\omega}_0, \tilde{\Omega})$ of bandwidth $\hat{\omega}_s = 2\omega_s$, where $\tilde{T}_p = N_{p2}\Delta t/2$, $\tilde{\omega}_0 = 1.5\omega_s$, and $\tilde{\Omega} = 0.5\omega_s$ (Figure 4). Because field rays constitute convolutions of source rays band limited to ω_s with $A_{pq}^{FW}(\mathbf{0}, \mathbf{0}, t)$, they are band limited to ω_s as well and hence can be represented by the same new APSWFs.

[25] With this background, a description of the blocked FFT scheme for evaluating temporal convolutions involving TDFW kernels becomes possible. For the sake of brevity, only the scheme's application to the construction of the scalar field rays is described. With minor modifications, the procedures outlined can be applied to the construction of vector field rays as well. It follows from the above discussion that samples of vector field ray (p, q) can be expressed in terms of a discrete convolution

$$F_{pq}^{\phi}(i'\Delta t/2) = \left\{ A_{pq}^{FW}(\mathbf{0}, \mathbf{0}, t) * \sum_{i=1}^{\lfloor i'/2 \rfloor} S_{pq,i}^{\phi}(t) \right\}_{t=i'\Delta t/2}$$
$$= \sum_{k'=1}^{i'} H_{pq}[(i' - k')\Delta t/2] \left[\sum_{i=1}^{\lfloor i'/2 \rfloor} S_{pq,i}^{\phi}(k'\Delta t/2) \right] \quad (24)$$

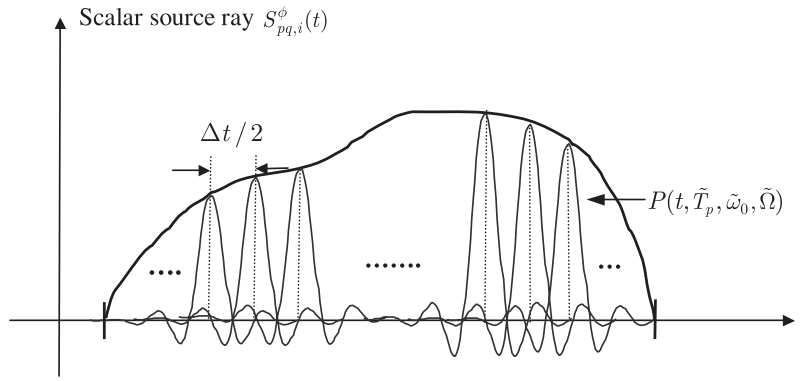

Figure 4. Reconstruction of the scalar source ray $S^{\phi}_{pq,i}(t)$ using a set of modified APSWFs $P(t, \tilde{T}_p, \tilde{\omega}_0, \tilde{\Omega})$.

for $i' = 1, \ldots, 2N_t$, where

$$H_{pq}(t) = P\big(t, \tilde{T}_p, \tilde{\omega}_0, \tilde{\Omega}\big) * A^{FW}_{pq}(\mathbf{0}, \mathbf{0}, t) = \int_{-\infty}^{+\infty} P\big(t', \tilde{T}_p, \tilde{\omega}_0, \tilde{\Omega}\big) A^{FW}_{pq}(\mathbf{0}, \mathbf{0}, t - t')dt'. \quad (25)$$

The first equality in (24) follows from (21) and (22). The second equality was obtained by expressing the source rays in terms of their samples associated with APSWF $P(t, \tilde{T}_p, \tilde{\omega}_0, \tilde{\Omega})$. The summation over k' in (24) can be split into two parts:

$$F^{\phi}_{pq}(i'\Delta t/2) = \sum_{k'=i'-N_{shift}}^{i'} H_{pq}[(i'-k')\Delta t/2] \cdot \left[\sum_{i=1}^{\lfloor i'/2\rfloor} S^{\phi}_{pq,i}(k'\Delta t/2)\right] + \sum_{k'=1}^{i'-N_{shift}-1} H_{pq}[(i'-k')\Delta t/2] \cdot \left[\sum_{i=1}^{\lfloor i'/2\rfloor} S^{\phi}_{pq,i}(k'\Delta t/2)\right], \quad (26)$$

where $N_{shift} = 2N_{del} + 2N_{pro} + 2N_{exc}$. This choice for N_{shift} guarantees that

$$\sum_{i=1}^{\lfloor i'/2\rfloor} S^{\phi}_{pq,i}(k'\Delta t/2) = S^{\phi}_{pq}(k'\Delta t/2) \quad (27)$$

when $k' \le i' - N_{shift} - 1$. (Please refer to Figure 5 for the temporal locations of the source rays at different time steps.) The first summation on the right hand side of (26) requires $O(1)$ operations for each i', and therefore a total of $O(N_t)$ operations for $i' = 1, \ldots, 2N_t$. The second summation in the right-hand side of (26) can be efficiently evaluated using the blocked FFT scheme as detailed next. First, it is noted that this sum can be expressed as a matrix-vector multiplication as

$$\sum_{k'=1}^{i'-N_{shift}-1} H_{pq}[(i'-k')\Delta t/2]\left[\sum_{i=1}^{\lfloor i'/2\rfloor} S^{\phi}_{pq,i}(k'\Delta t/2)\right] = \sum_{k'=1}^{i'-N_{shift}-1} H_{pq}[(i'-k')\Delta t/2] S^{\phi}_{pq}(k'\Delta t/2) = \bar{\mathbf{H}}_{pq}\mathbf{B}_{pq} \quad (28)$$

for $i' = 1, \ldots, 2N_t$, where the vector $\mathbf{B}_{pq}$ is of dimension $2N_t$ and contains elements

$$\big[\mathbf{B}_{pq}\big]_{k'} = S^{\phi}_{pq}(k'\Delta t/2), k' = 1, \ldots, 2N_t, \quad (29)$$

while the $\bar{\mathbf{H}}_{pq}$ is a matrix of dimension $2N_t \times 2N_t$ with elements (Figure 6)

$$\big[\bar{\mathbf{H}}_{pq}\big]_{i'k'} = \begin{cases} H_{pq}[(i'-k')\Delta t/2] & i' \ge k' + N_{shift} + 1 \\ 0 & i' < k' + N_{shift} + 1 \end{cases}, \quad i', k' = 1, \ldots, 2N_t. \quad (30)$$

Samples of $H_{pq}(t)$ can be calculated and stored before the MOT process starts. Equation (28) should be evaluated in the context of the MOT. This implies that, the convolutional nature of (28) notwithstanding, a straightforward FFT cannot be used to evaluate the $F^{\phi}_{pq}(i'\Delta t/2)$ because source rays $S^{\phi}_{pq,\lfloor i'/2\rfloor}(t)$, $S^{\phi}_{pq,\lfloor i'/2\rfloor+1}(t)$, ... are not available yet. Therefore the convolution in (28) is evaluated using so-called blocked FFTs (proposed by *Harrier et al.* [1985], with the purpose of accelerating temporal convolutions when solving Volterra integral equations), that allow fields produced by currents to become available for the purpose of advancing the MOT process without requiring FFTs of full length $2N_t$ each and every time step. To this end, as shown in Figure 6b,

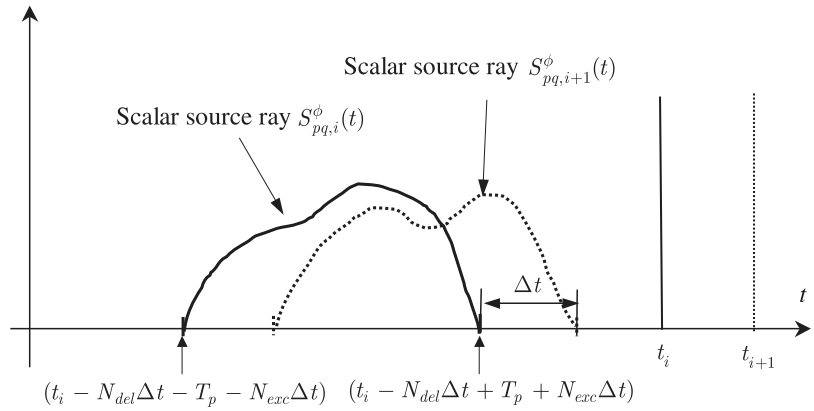

Figure 5. Illustration of the scalar source rays at two different time steps. Note that the width of the scalar source ray is fixed at different time steps.

the part of matrix $\bar{\mathbf{H}}_{pq}$ that is covered by nonzero elements is subdivided into blocks, each of which can be multiplied with the corresponding part of the vector $\mathbf{B}_{pq}$ using a simple (nonblocked) FFT, within the framework of MOT. The reader is referred to *Yilmaz et al.* [2002] for the details of the scheme, and a proof of the fact that the cost of the resulting scheme scales as $O(N_t \log^2 N_t)$.

[26] Although the above presentation focused on planar PEC structures, it is easily extended to the case of discretely planar structures, viz. scatterers comprising a finite number of (offset) planar screens. The required modifications to the algorithm involve the construction of TDFW representations and corresponding blocked FFT accelerators for all pairs of interacting screens. This renders the scheme impractical when the number of screens becomes large, or, equivalently, when a continuum of source and observation planes exists, as is the case when studying scattering from substrate imprinted structures.

3. Numerical Results

[27] This section presents several numerical results that demonstrate the capabilities of the above-described Floquet wave–based MOT (FW-MOT) solver. All results obtained with the FW-MOT code were compared against data from a periodic frequency domain method of moments (P-MOM) code following Fourier transformation of the time domain currents/fields to the frequency domain. All periodic structures considered below are illuminated by an electric field $\mathbf{E}^{inc}(\mathbf{r}, t, \hat{\mathbf{p}}^{inc}) = \hat{\mathbf{p}}^{inc} f(t - \hat{\mathbf{k}}^{inc} \cdot \mathbf{r}/c)$ with $f(t)$ a modulated Gaussian pulse parametrized as

$$f(t) = \cos\left[2\pi f_c (t - t_p)\right] \exp\left[-(t - t_p)^2/(2\sigma^2)\right], \quad (31)$$

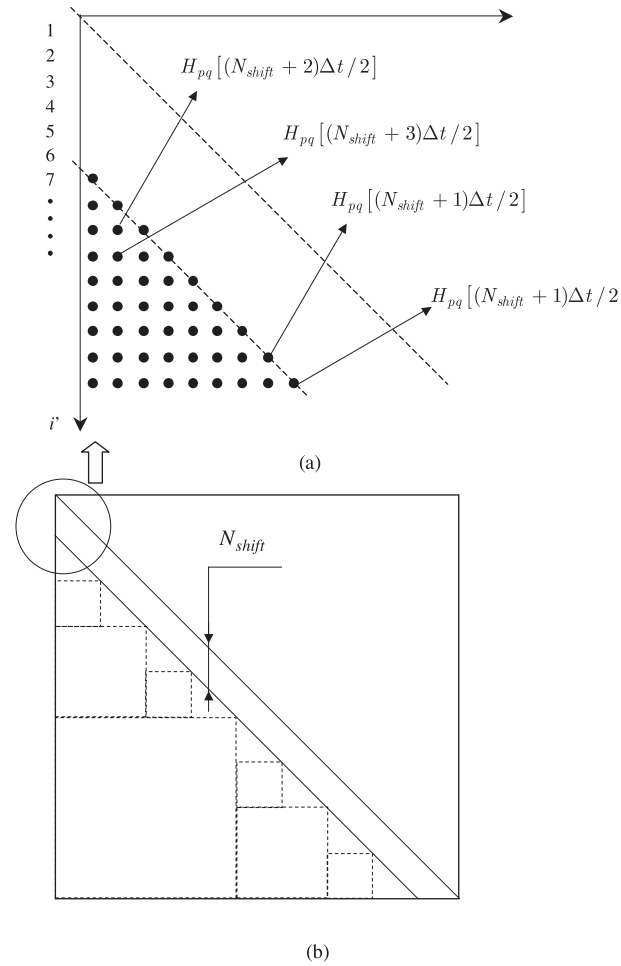

Figure 6. (a) Illustration of the matrix $\bar{\mathbf{H}}_{pq}$. (b) Schematic diagram of the acceleration of the matrix vector multiplication using a blocked FFT scheme.

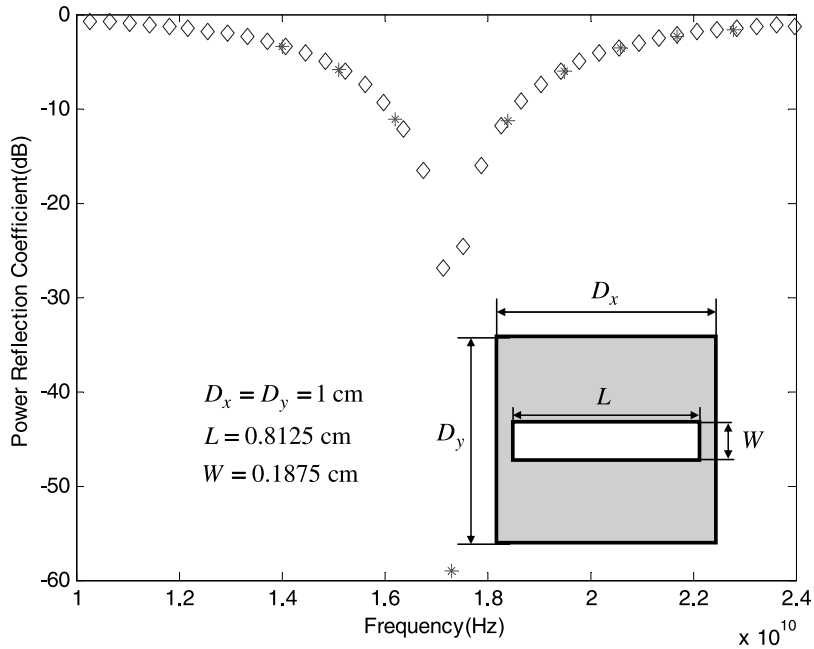

Figure 7. Power reflection coefficients for a slot element at normal incident case (P-MOM, asterisks; FW-MOT, diamonds).

where f_c is center frequency of the incident wave, $\sigma = 3/(2\pi f_{bw})$ and $t_p = 6\sigma$ with f_{bw} termed the "bandwidth" of the signal.

[28] The first structure analyzed comprises periodically arranged rectangular slots in a PEC ground plane (Figure 7). The side length of the square mothercell is 1 cm. The dimension of the slot is shown in the inset of Figure 7. Current on the slotted ground plane is described in terms of $N_s = 1032$ spatial unknowns. The incident pulse has $\hat{\mathbf{k}}^{inc} = -\hat{\mathbf{z}}$, $\hat{\mathbf{p}}^{inc} = \hat{\mathbf{y}}$, $f_c = 15$ GHz, and $f_{bw} = 11$ GHz. The time step is $\Delta t = 2.564$ ps and the number of time steps $N_t = 1024$. The number of Floquet modes N_{mod} of 69 is used for the FW-MOT scheme. The power reflection coefficients [*Chen et al.*, 2003] for the structure obtained via the FW-MOT scheme and P-MOM scheme are compared in Figure 7. Excellent agreement between the two data sets is observed.

[29] Next, the structure analyzed comprises periodically arranged Minkowski patches studied by *Gianvittorio et al.* [2001]. This patch is designed to resonate in two separate frequency bands. The side length of the square mothercell is 30 cm. The dimension of the patch is shown in the inset of Figure 8. Current on the patch is discretized in terms of $N_s = 2166$ spatial unknowns. The incident pulse has $\hat{\mathbf{k}}^{inc} = -\hat{\mathbf{z}}$, $\hat{\mathbf{p}}^{inc} = \hat{\mathbf{x}}$, $f_c = 1.25$ GHz, and $f_{bw} = 1.25$ GHz. The time step is $\Delta t = 22.22$ ps and the number of time steps $N_t = 2048$. It is noted that in this example the dimensions of the mothercell measured at the sampling frequency $\omega_s = \pi/\Delta t$ are considerably larger than those used in the last example (by approximately a factor of ten). As a result, $N_{\text{mod}} = 799$ Floquet modes have to be used in the FW-MOT solver. The power transmission coefficients [*Chen et al.*, 2003] for the structure obtained using the FW-MOT scheme and P-MOM scheme are compared in Figure 8. As expected, two nulls corresponding to the resonances of the big and small square patch elements, respectively, are observed. The results obtained using the FW-MOT and P-MOM codes agree very well.

[30] The third structure analyzed comprises periodically arranged four-legged elements which are loaded with PEC patches and lumped elements [*Epp*, 1990]. The side length of the square mothercell is 1 cm and the dimension of the four-legged element is shown in the inset of Figure 9. As shown in the inset of Figure 9, each of the center cross' two legs is connected to the PEC patch through a parallel RLC resonant circuit with R = 1000 Ω, L = 1.3 nH, and C = 0.1 pF, which is marked as a shaded square. Current on the four-legged element and the PEC patch is discretized in terms of $N_s = 383$ spatial unknowns. The incident pulse has $\hat{\mathbf{k}}^{inc} = -\hat{\mathbf{z}}$, $\hat{\mathbf{p}}^{inc} = \hat{\mathbf{x}}$, $f_c = 15$ GHz, and $f_{bw} = 15$ GHz. The time step is $\Delta t = 2.22$ ps and the number of time steps $N_t = 1024$. The number of Floquet modes N_{mod} of 61 is used for the FW-MOT scheme. The power reflection coefficients of the structure obtained using the FW-MOT scheme and

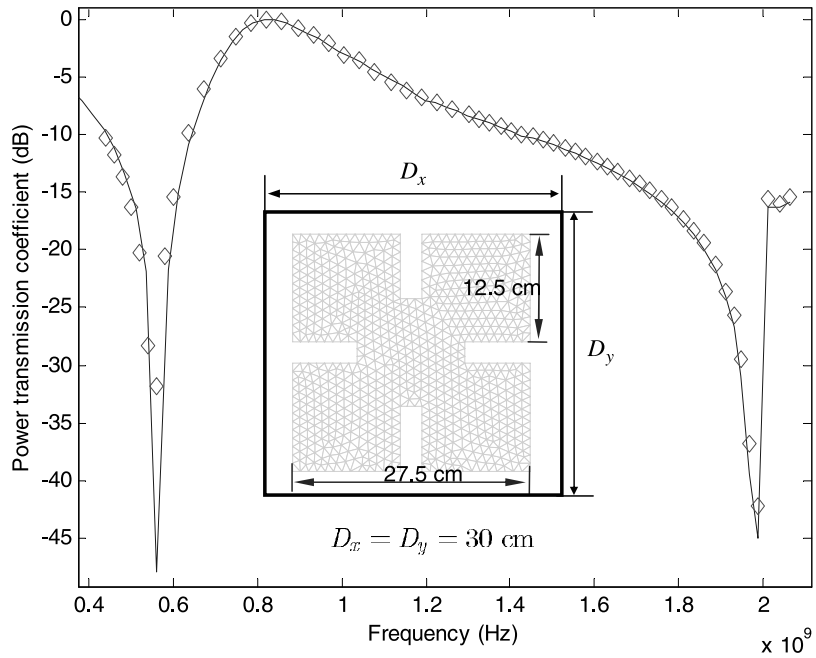

Figure 8. Power transmission coefficients for a fractal element at normal incident case (P-MOM, diamonds; FW-MOT, solid line).

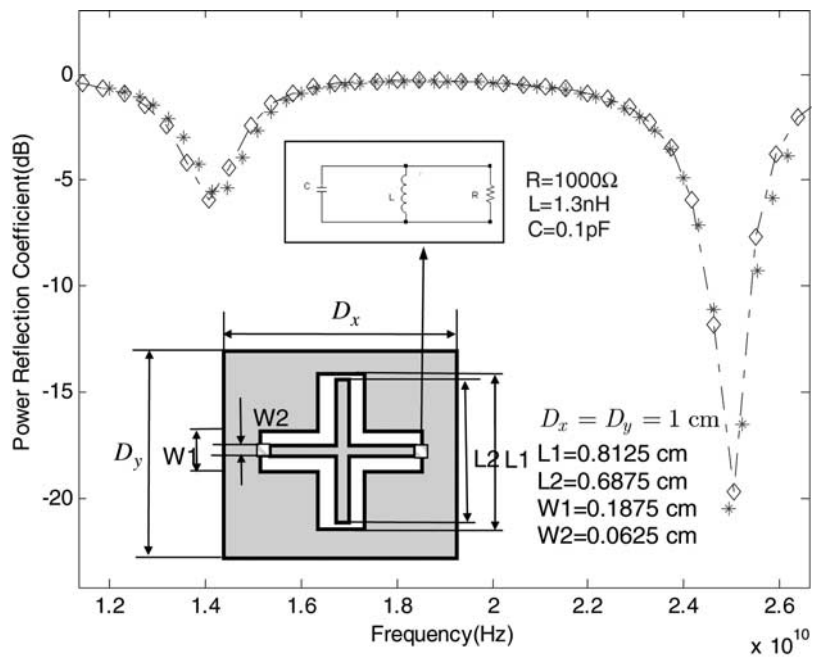

Figure 9. Power reflection coefficients for a four-legged element at normal incident case (P-MOM, asterisks; FW-MOT, dashed line with diamonds).

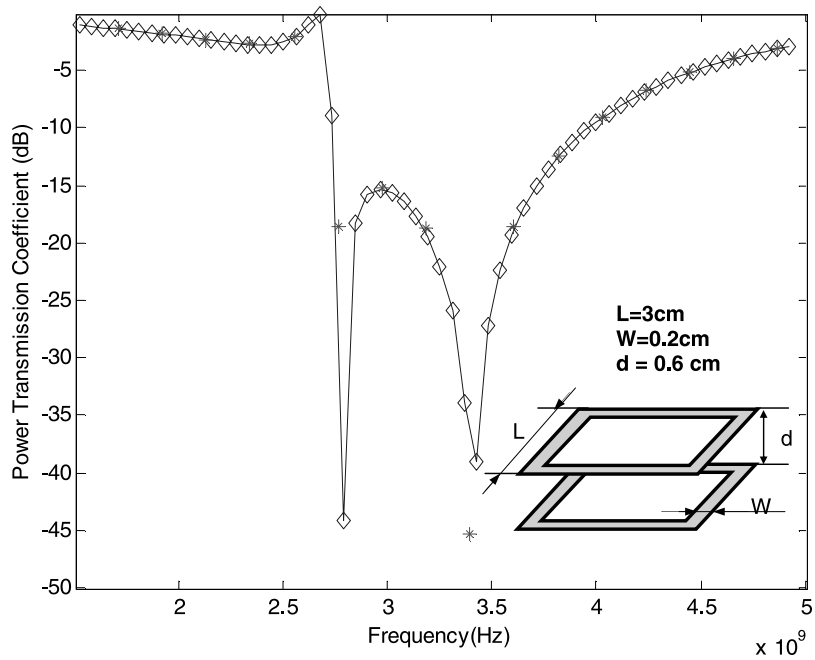

Figure 10. Power transmission coefficients for a dual-screen square loop element at normal incident case (P-MOM, asterisks; FW-MOT, solid line with diamonds).

P-MOM scheme are compared in Figure 9. The two nulls around 14GHz and 25GHz corresponding to the resonances of the structures while the RLC resonant circuits are removed or replaced with PEC patches respectively are observed in the power reflection coefficients plot. Again, TD-MOT and P-MOM results are in good agreement.

[31] Finally, a two screen structure comprising periodically arranged identical square loop elements is analyzed. The side length of the square mothercell is 4 cm. The dimensions of the square loop are defined in the inset of Figure 10. Current on the dual square loop elements is discretized in terms of N_s = 224 spatial unknowns. The incident pulse has $\hat{\mathbf{k}}^{inc} = -\hat{\mathbf{z}}$, $\hat{\mathbf{p}}^{inc} = \hat{\mathbf{x}}$, f_c = 3 GHz, and f_{bw} = 3 GHz. The time step is Δt = 8.33 ps and the number of time steps N_t = 1024. The number of Floquet modes N_{mod} of 99 is used for the FW-MOT scheme. The power transmission coefficients plot for the structure obtained via the FW-MOT scheme and P-MOM scheme are shown in Figure 10 and agree excellently.

4. Conclusions

[32] A TDFW accelerated MOT-based scheme pertinent to the analysis of transient scattering from doubly periodic, discretely planar, PEC structures was presented. The TDFW concepts were employed to efficiently represent the fields generated by periodic arrangements of discretely planar source constellations. APSWFs were chosen as temporal basis functions in the proposed solver because of their interpolatory and spectral properties, and the convolution of the TDFW kernel with the periodic structure currents was accelerated using a blocked FFT scheme. Even though application of the scheme is restricted to discretely planar structures, it has many applications, some of which were demonstrated in this paper. The proposed scheme was validated through comparison of scattering data for various periodic structures against frequency domain results. Current research focuses on the use of this method in the construction of hybrid time domain boundary integral—finite element schemes for analyzing transient scattering from penetrable periodic structures (in which the boundary integrals are confined to two parallel interfaces and the present scheme is directly applicable) and on developing a Floquet wave–based solver that permits efficient means for analyzing transient scattering from nonplanar doubly periodic structures.

Appendix A: Truncation of the TDFW Series

[33] This appendix demonstrates that, when the periodic time domain Green's function $G(\boldsymbol{\rho}, \boldsymbol{\rho}', t)$ is convolved with the (approximately) time- and (strictly) band-limited APSWF $P(t, T_p, \omega_0, \Omega)$, then only the "not deeply evanescent TDFWs" significantly contribute to the resulting field "shortly after $P(t, T_p, \omega_0, \Omega)$

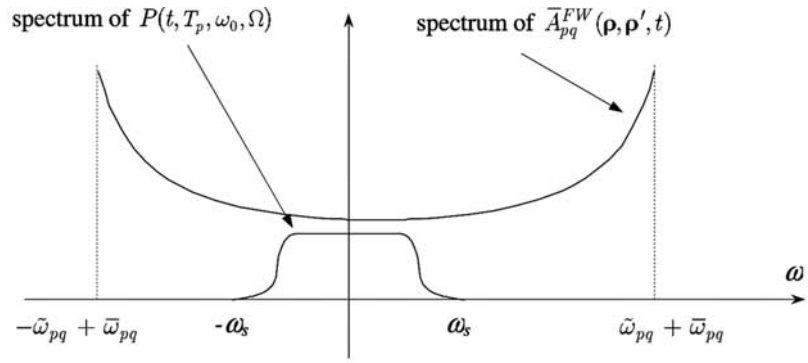

Figure A1. Illustration of the spectra of $P(t, T_p, \omega_0, \Omega)$ and $\bar{A}_{pq}^{FW}(\rho, \rho', t)$.

vanishes." A more intuitive, though only qualitative, demonstration was given by *Capolino and Felsen* [2003] on the basis of the excitation of local instantaneous frequencies of the various A_{pq}^{FW}.

[34] Before firming up the above statement, some preliminary comments are in order. (1) The TDFW $A_{pq}^{FW}(\rho, \rho', t)$ in (16) can be expressed as

$$A_{pq}^{FW}(\rho, \rho', t) = \bar{A}_{pq}^{FW}(\rho, \rho', t)U(t - t_0), \tag{A1}$$

where

$$\bar{A}_{pq}^{FW}(\rho, \rho', t) = \gamma e^{j\bar{\omega}_{pq}\tau} J_0\left[\tilde{\omega}_{pq}(t - t_0)\right] \tag{A2}$$

and $\gamma = ce^{-j\alpha_{pq}\cdot(\rho-\rho')}/2D_xD_y\sqrt{1-\eta^2}$. Below, the convolution $\bar{A}_{pq}^{FW}(\rho, \rho', t) * P(t, T_p, \omega_0, \Omega)$ will be studied first; conclusion reached will be extended to $A_{pq}^{FW}(\rho, \rho', t) * P(t, T_p, \omega_0, \Omega)$ thereafter. (2) The Fourier transform of $\bar{A}_{pq}^{FW}(\rho, \rho', t)$ is (Figure A1) [*Gradshteyn and Ryzhik*, 1980]

$$\mathcal{F}\left\{\bar{A}_{pq}^{FW}(\rho, \rho', t)\right\} = \int_{-\infty}^{+\infty} \bar{A}_{pq}^{FW}(\rho, \rho', t)e^{-j\omega t}dt = \begin{cases} \dfrac{(2\gamma)e^{-j\omega t_0}}{\sqrt{\tilde{\omega}_{pq}^2 - (\omega - \bar{\omega}_{pq})^2}} & \omega \in (-\tilde{\omega}_{pq} + \bar{\omega}_{pq}, \tilde{\omega}_{pq} + \bar{\omega}_{pq}) \\ 0 & \text{elsewhere} \end{cases}. \tag{A3}$$

The spectrum of $\bar{A}_{pq}^{FW}(\rho, \rho', t)$ is nonzero only for $\omega \in (-\tilde{\omega}_{pq} + \bar{\omega}_{pq}, \tilde{\omega}_{pq} + \bar{\omega}_{pq})$; it follows from (17) that both $|-\tilde{\omega}_{pq} + \bar{\omega}_{pq}|$ and $|\tilde{\omega}_{pq} + \bar{\omega}_{pq}|$ grow and that the spectrum of $\bar{A}_{pq}^{FW}(\rho, \rho', t)$ becomes increasingly smooth around $\omega = 0$ as $|p|$ and/or $|q|$ increase. Note however that (A3) is not the spectrum of A_{pq}^{FW}. (3) The Fourier transform of $P(t, T_p, \omega_0, \Omega)$ is nonzero only for $\omega \in (-\omega_s, \omega_s)$ with $\omega_s = \omega_0 + \Omega$ (Figure A1); $P(t, T_p, \omega_0, \Omega)$ itself is vanishingly small outside the temporal interval $(-T_p, T_p)$. (4) The dimensionless parameters $\xi_{pq}^{\min}_{\max} = \min_{\max}(|-\bar{\omega}_{pq}/\omega_s + \tilde{\omega}_{pq}/\omega_s|, |\tilde{\omega}_{pq}/\omega_s + \bar{\omega}_{pq}/\omega_s|)$ measure the position of the spectra of $\bar{A}_{pq}^{FW}(\rho, \rho', t)$ and $P(t, T_p, \omega_0, \Omega)$ relative to one another. The parameter $\xi_{pq}^{\min}$ is especially important. Modes (p, q) with $\xi_{pq}^{\min} > 1$ are termed evanescent; for these modes $P(t, T_p, \omega_0, \Omega)$'s spectral support is fully contained within that of $\bar{A}_{pq}^{FW}(\rho, \rho', t)$ —this situation is depicted in Figure A1. Modes (p, q) with $\xi_{pq}^{\min} < 1$ are termed propagating; for these modes $P(t, T_p, \omega_0, \Omega)$'s spectral support resides partially outside that of $\bar{A}_{pq}^{FW}(\rho, \rho', t)$. The discussion below pertains only to evanescent modes.

[35] A partially computational demonstration of this appendix' opening statement based on the fact that the spectra of TDFWs are increasingly smooth in the interval $\omega \in (-\omega_s, \omega_s)$ for larger $\xi_{pq}^{\min}$, is presented next. Assume that there exists a time-limited function $B(t)$ with spectrum that approaches that of $\bar{A}_{pq}^{FW}(\rho, \rho', t)$ for $\omega \in (-\omega_s, \omega_s)$ and with energy not exceeding that of $\bar{A}_{pq}^{FW}(\rho, \rho', t)$ restricted to the same interval by a fixed and small multiplicative constant c_1 (typically < 10):

$$\mathcal{F}\left\{\bar{A}_{pq}^{FW}(\rho, \rho', t)\right\} \approx \mathcal{F}\{B(t)\} \quad \text{for} \quad \omega \in (-\omega_s, \omega_s) \tag{A4a}$$

$$\| B(t) \| / \int_{-\omega_s}^{\omega_s} \left|\mathcal{F}\left\{\bar{A}_{pq}^{FW}(\rho, \rho', t)\right\}\right|^2 d\omega < c_1. \tag{A4b}$$

The fact that $P(t, T_p, \omega_0, \Omega)$ is band limited to $(-\omega_s, \omega_s)$ along with (A4a) ensure that

$$\bar{A}_{pq}^{FW}(\rho, \rho', t) * P\left(t, T_p, \omega_0, \Omega\right) \approx B(t) * P\left(t, T_p, \omega_0, \Omega\right). \tag{A5}$$

Equation (A5), along with the fact that $P(t, T_p, \omega_0, \Omega)$ is approximately time limited and (A4b) guarantee that $B(t) * P(t, T_p, \omega_0, \Omega)$ and $\bar{A}_{pq}^{FW}(\rho, \rho', t) * P(t, T_p, \omega_0, \Omega)$ are

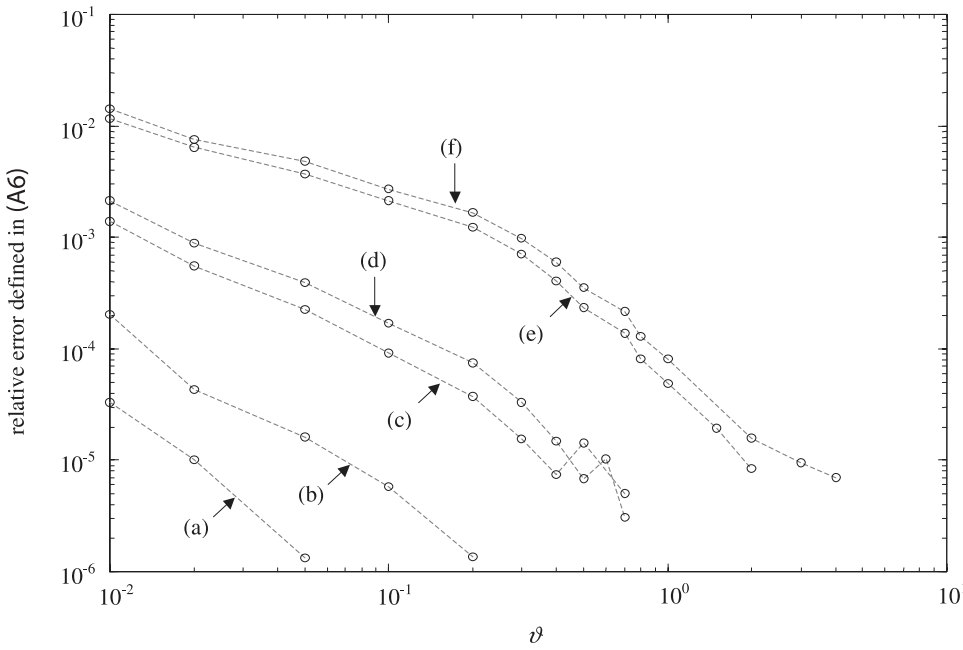

Figure A2. Relative error when approximating the spectrum of $\bar{A}_{pq}^{FW}(\boldsymbol{\rho}, \boldsymbol{\rho}', t)$: for line a $\xi_{pq}^{\min} = 2.5$ and $\xi_{pq}^{\max} = 2.5$; for line b $\xi_{pq}^{\min} = 1.8$ and $\xi_{pq}^{\max} = 2.2$; for line c $\xi_{pq}^{\min} = 1.4$ and $\xi_{pq}^{\max} = 2.6$; for line d $\xi_{pq}^{\min} = 4/3$ and $\xi_{pq}^{\max} = 2$; for line e $\xi_{pq}^{\min} = 8/7$ and $\xi_{pq}^{\max} = 12/7$; and for line f $\xi_{pq}^{\min} = 9/8$ and $\xi_{pq}^{\max} = 11/8$.

approximately time limited too – condition (35b) ensures that out-of-band spectral components that arise upon time limiting $P(t, T_p, \omega_0, \Omega)$ to $(-T_p, T_p)$ in a computational setting do not destroy (A5). Next, it is shown that, for modes with large enough $\xi_{pq}^{\min} > 1$, there exist $B(t)$ for which (A4a) holds to arbitrary accuracy. To this end, $B(t)$ is assumed of the form $B(t) = \sum_{n=1}^{N} B_n \delta(t - t_n)$; here the t_n are sampled uniformly in between $-\vartheta\Delta t + t_0$ and $\vartheta\Delta t + t_0$ ($\Delta t = \pi/\omega_s$) and the coefficients B_n, $n = 1, \ldots, N$ are determined by enforcing (A4a) in a least squares sense while restricting $B(t)$'s energy according to (A4b). The relative error in (A4a) is defined as

$$\left(\frac{\int_{-\omega_s}^{\omega_s} \left| \mathcal{F}\left\{ \bar{A}_{pq}^{FW}(\boldsymbol{\rho}, \boldsymbol{\rho}', t) \right\} - \sum_{n=1}^{N} B_n e^{-j\omega t_n} \right|^2 d\omega}{\int_{-\omega_s}^{\omega_s} \left| \mathcal{F}\left\{ \bar{A}_{pq}^{FW}(\boldsymbol{\rho}, \boldsymbol{\rho}', t) \right\} \right|^2 d\omega} \right)^{1/2}, \tag{A6}$$

and only depends on the dimensionless parameters $\xi_{pq}^{\min}$, $\xi_{pq}^{\max}$, and ϑ. Figure A2 shows that for evanescent modes with sufficiently large $\xi_{pq}^{\min} > 1$ the relative error decreases exponentially fast with ϑ. For all cases shown in Figure A2, the relative error reduces to less than 10^{-5} when ϑ is larger than 4. For a fixed ϑ, the relative error decreases exponentially fast with $\xi_{pq}^{\min}$ and, understandably, is insensitive to $\xi_{pq}^{\max}$. In conclusion, when $\xi_{pq}^{\min}$ is sufficiently large, then a well-behaved function $B(t)$ that is nonzero only for $t \in [-\vartheta\Delta t + t_0, \vartheta\Delta t + t_0]$ can be constructed such that $\mathcal{F}\{\bar{A}_{pq}^{FW}(\boldsymbol{\rho}, \boldsymbol{\rho}', t)\} \approx \mathcal{F}\{B(t)\}$ for $\omega \in (-\omega_s, \omega_s)$. It follows that $B(t) * P(t, T_p, \omega_0, \Omega)$ is time limited to within $t \in (-T_p - \vartheta\Delta t + t_0, T_p + \vartheta\Delta t + t_0)$ and therefore that $\bar{A}_{pq}^{FW}(\boldsymbol{\rho}, \boldsymbol{\rho}', t) * P(t, T_p, \omega_0, \Omega) \approx 0$ when $t > T_p + \vartheta\Delta t + t_0$. Using (A1) it follows that

$$\begin{aligned} A_{pq}^{FW}(\boldsymbol{\rho}, \boldsymbol{\rho}', t) * P(t, T_p, \omega_0, \Omega) &\approx \int_{-T_p}^{T_p} dt' P(t', T_p, \omega_0, \Omega) \\ &\cdot A_{pq}^{FW}(\boldsymbol{\rho}, \boldsymbol{\rho}', t - t') \overset{t > T_p + t_0}{=} \int_{-T_p}^{T_p} dt' P(t', T_p, \omega_0, \Omega) \\ &\cdot \bar{A}_{pq}^{FW}(\boldsymbol{\rho}, \boldsymbol{\rho}', t - t') = \bar{A}_{pq}^{FW}(\boldsymbol{\rho}, \boldsymbol{\rho}', t) * P(t, T_p, \omega_0, \Omega). \end{aligned} \tag{A7}$$

Hence

$$A_{pq}^{FW}(\boldsymbol{\rho}, \boldsymbol{\rho}', t) * P(t, T_p, \omega_0, \Omega) \approx 0 \tag{A8}$$

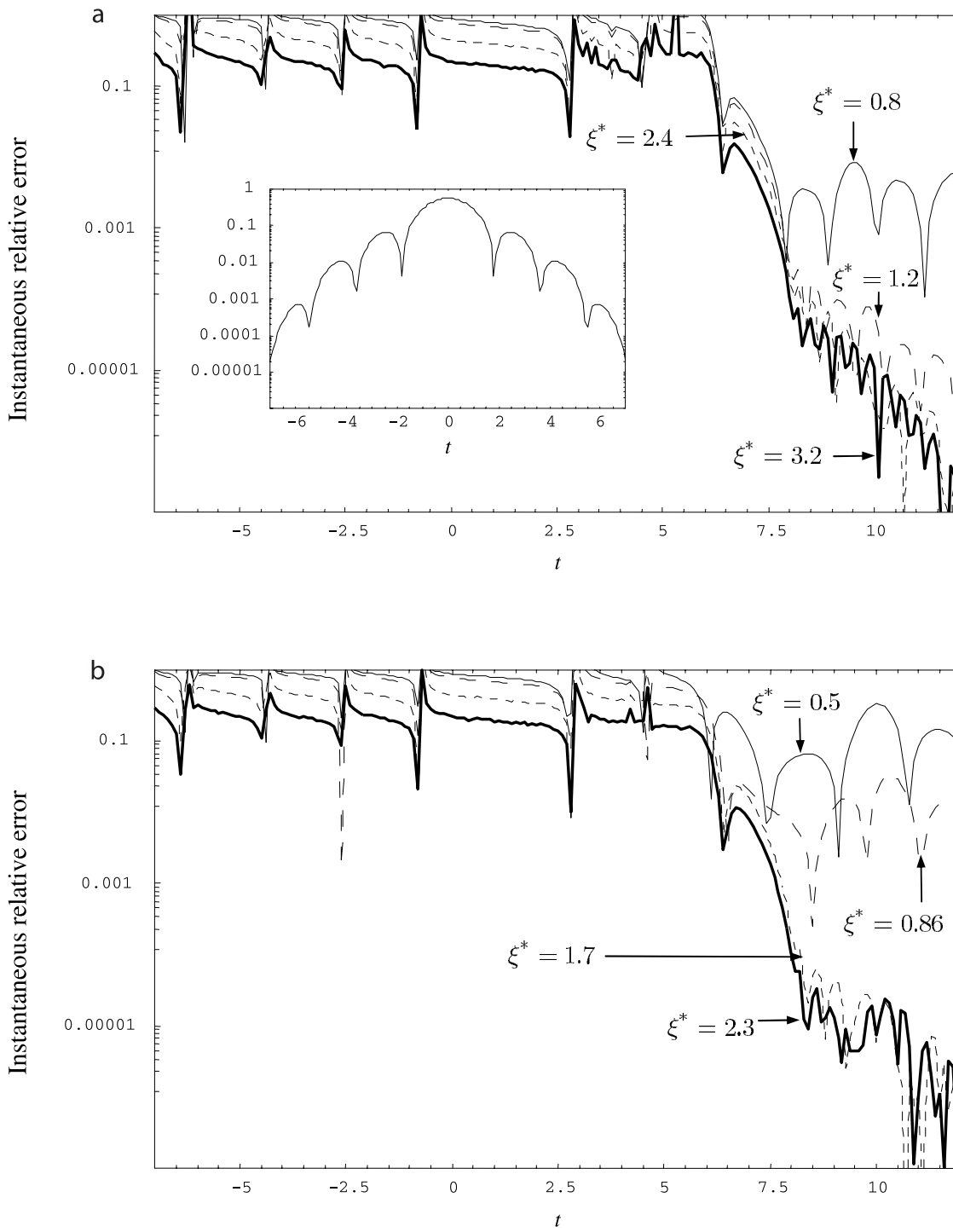

Figure A3. Instantaneous error due to the truncation of TDFWs.

when $\xi_{pq}^{\min}$ is sufficiently larger than one and $t > T_p + \vartheta\Delta t + t_0$. A direct consequence of (A8) is that, when the time domain periodic Green's function is convolved with an APSWF, the high-order Floquet waves do not contribute if the convolution is observed for $t > T_p + \vartheta\Delta t + t_0$. In other words, in

$$\begin{aligned} & G(\boldsymbol{\rho}, \boldsymbol{\rho}', t) * P\left(t, T_p, \omega_0, \Omega\right) \\ & = \sum_{m=-\infty}^{m=+\infty} \sum_{n=-\infty}^{n=+\infty} \frac{\delta\left(t - \hat{\mathbf{k}}^{inc} \cdot \boldsymbol{\rho}_{mn}^{c}/c - \left|\boldsymbol{\rho}' + \boldsymbol{\rho}_{mn}^{c} - \boldsymbol{\rho}\right|/c\right)}{\left|\boldsymbol{\rho}' + \boldsymbol{\rho}_{mn}^{c} - \boldsymbol{\rho}\right|} \\ & * P\left(t, T_p, \omega_0, \Omega\right) \quad \approx \sum_{\left\{(p,q), \xi_{pq}^{\min} \le \xi^*\right\}} A_{pq}^{FW}(\boldsymbol{\rho}, \boldsymbol{\rho}', t) \\ & * P\left(t, T_p, \omega_0, \Omega\right), \end{aligned}$$

the error in the TDFW expansion rapidly tends to zero as ξ^* increases beyond unity and $t > T_p + \vartheta\Delta t + t_0$. It is easily verified that, for a fixed ξ^*, the number of TDFWs for which $\xi_{pq}^{\min} \le \xi^*$ is proportional to the area of the mother cell measured in wavelengths at the sampling frequency $\omega_s = \pi/\Delta t$. To be specific, if the total number of TDFWs that satisfies $\xi_{pq}^{\min} \le \xi^*$ is denoted as N_{mod}, then $N_{\text{mod}} \propto D_x D_y (\xi^* \omega_s / c)^2$. The convergence of the truncated TDFW series (A9) is verified numerically through one example with $\Delta t = 1$ s, $\omega_0 = 0.55\pi$ rad/s, $\Omega = 0.45\pi$ rad/s, $T_p = 7$ s, $\omega_s = \omega_0 + \Omega = \pi$ rad/s, $D_x = D_y = 7c\Delta t$, $\boldsymbol{\rho} = (0.0, 0.00001 D_x)$ and $\boldsymbol{\rho}' = (0.0, 0.0)$. Figure A3 show the instantaneous relative error in (A9), for various choices of ξ^*. In Figures A3a and A3b, $\hat{\mathbf{k}}^{inc} = \hat{\mathbf{z}}$ and $\hat{\mathbf{k}}^{inc} = \hat{\mathbf{x}}(1/2) + \hat{\mathbf{z}}(\sqrt{3}/2)$, respectively. The waveform of the APSWF is also plotted in the inset of Figure A3a. It is observed the APSWF virtually vanishes after time T_p. The relative error for $t < T_p$ is always large, irrespective of the choice of ξ^*. When ξ^* is smaller than 1, the relative error remains large, even for $t > T_p$. However, when ξ^* is chosen greater than 1, the relative error becomes vanishingly small for $t > T_p$.

[36] **Acknowledgment.** This research was supported in part by ARO grant DAAD19-00-1-0464, the DARPA VET Program under contract F49620-01-1-0228, MURI grant F49620-01-1-04 "Analysis and design of ultra-wide band and high power microwave pulse interactions with electronic circuits and systems," and the NSF under CCR: 9988347 and 0306436.

References

Aygün, K., M. Lu, B. Shanker, and E. Michielssen (2000), Analysis of PCB level EMI phenomena using an adaptive low-frequency plane wave time domain algorithm, paper presented at 2000 International Symposium on Electromagnetic Compatibility, Inst. of Electr. and Electron. Eng., Washington D. C., 21–25 Aug.

Bleszynski, E., M. Bleszynski, and T. Jaroszewicz (2001), A new fast time domain integral equation solution algorithm, in *IEEE Antennas and Propagation Society International Symposium 2001*, vol. 4, pp. 176–179, IEEE Press, Piscataway, N. J.

Cadzow, J. A. (1979), An extrapolation procedure for band-limited signals, *IEEE Trans. Acoust. Speech Signal Process.*, *27*, 4–12.

Capolino, F., and L. Felsen (2002), Frequency- and time-domain Green's function for a phased semi-infinite periodic line array of dipoles, *IEEE Trans. Antennas Propag.*, *50*, 31–34.

Capolino, F., and L. Felsen (2003), Time-domain Green's function for an infinite sequentially excited periodic planar array of dipoles, *IEEE Trans. Antennas Propag.*, *51*, 160–170.

Chen, N.-W., B. Shanker, and E. Michielssen (2002), Volume/surface-integral-equation-based analysis of transient scattering from periodic perfectly conducting structures with dielectric media, paper presented at National Radio Science Meeting, U.S. Natl. Comm. of the Int. Union of Radio Sci., San Antonio, Tex.

Chen, N.-W., B. Shanker, and E. Michielssen (2003), Integral-equation-based analysis of transient scattering from doubly periodic perfectly conducting structures, *IEE Proc., Part H, Microwave Antennas Propag.*, *150*, 120–124.

Epp, L. W. (1990), Frequency selective surfaces with lumped and time-varying loads, variable surface impedance and multiple screens, Ph.D. dissertation, Univ. of Ill. at Urbana-Champaign, Urbana.

Ergin, A. A., B. Shanker, and E. Michielssen (1998), Fast evaluation of three-dimensional transient wave fields using diagonal translation operators, *J. Comput. Phys.*, *146*, 157–180.

Felsen, L., and F. Capolino (2000), Time-domain Green's function for an infinite sequentially excited periodic line array of dipoles, *IEEE Trans. Antennas Propag.*, *48*, 921–931.

Gianvittorio, J. P., Y. Rahmat-Samii, and J. Romeu (2001), Fractal FSS: Various self-similar geometries used for dual-band and dual-polarized FSS, in *IEEE Antennas and Propagation Society International Symposium 2001*, vol. 3, pp. 640–643, IEEE Press, Piscataway, N. J.

Gradshteyn, I. S., and I. M. Ryzhik (1980), *Table of Integrals, Series, and Products*, Elsevier, New York.

Harms, P., and R. Mittra (1994), Implementation of the periodic boundary condition in the finite-difference time-domain algorithm for FSS structure, *IEEE Trans. Antennas Propag.*, *42*, 1317–1324.

Harrier, E., C. Lubich, and M. Schlichte (1985), Fast numerical solution of nonlinear Volterra convolution equations, *SIAM J. Sci. Stat. Comput.*, *6*, 532–541.

Holter, H., and H. Steyskal (2002), Infinite phased-array analysis using FDTD periodic boundary conditions—Pulse scanning in oblique directions, *IEEE Trans. Antennas Propag.*, *47*, 1508–1514.

Jordan, K. E., G. R. Richter, and P. Sheng (1986), An efficient numerical evaluation of the Green's function for the Helmholtz operator on periodic surfaces, *J. Comput. Phys.*, *63*, 222–235.

Jorgenson, R. E., and R. Mittra (1991), Scattering from structured slabs having two-dimensional periodicity, *IEEE Trans. Antennas Propag.*, *39*, 151–157.

Knab, J. J. (1979), Interpolation of bandlimited functions using the approximate prolate series, *IEEE Trans. Inf. Theory*, *25*, 717–720.

Maloney, J. G., and M. P. Kesler (2002), Analysis of periodic structures, in *Computational Electrodynamics: The Finite-Difference Time-Domain Method*, 2nd ed., edited by A. Taflove and S. C. Hagness, pp. 569–625, Artech House, Norwood, Mass.

Marrocco, G., and F. Capolino (2002), Transient radiation by periodic structures: Accuracy of the (time domain-floquet wave)–FDTD algorithm, in *IEEE Antennas and Propagation Society International Symposium 2002*, vol. 3, pp. 643–646, IEEE Press, Piscataway, N. J.

Rao, S. M., D. R. Wilton, and A. W. Glisson (1982), Electromagnetic scattering by surfaces of arbitrary shape, *IEEE Trans. Antennas Propag.*, *3*, 409–418.

Roden, J. A., S. D. Gedeny, M. P. Kesler, J. G. Maloney, and P. H. Harms (1998), Time-domain analysis of periodic structures at oblique incidence: Orthogonal and nonorthogonal FDTD implementations, *IEEE Trans. Microwave Theory Tech.*, *46*, 420–427.

Saad, Y. (1996), *Iterative Methods for Sparse Linear Systems*, PWS, New York.

Slepian, D., and H. O. Pollak (1961), Prolate spheroidal wave functions, Fourier analysis and uncertainty—I, *Bell Syst. Tech. J.*, 43–63, Jan.

Tsay, W. J., and D. M. Pozar (1993), Application of the FDTD technique to periodic problems in scattering and radiation, *IEEE Microwave Guided Wave Lett.*, *3*, 250–252.

Veysoglu, M. E., R. T. Shin, and J. A. Kong (1993), A finite-difference time-domain analysis of wave scattering from periodic surfaces: Oblique incidence case, *J. Electromagn. Waves Appl.*, *7*, 1595–1607.

Yee, K. S. (1996), Numerical solution of initial boundary value problems involving Maxwell's equations in isotropic media, *IEEE Trans. Antennas Propag.*, *14*, 302–307.

Yilmaz, A. E., D. S. Weile, B. Shanker, J.-M. Jin, and E. Michielssen (2002), Fast analysis of transient scattering in lossy media, *IEEE Antennas Wireless Propag. Lett.*, *1*, 14–17.

Yilmaz, A. E., J.-M. Jin, and E. Michielssen (2003), Time domain adaptive integral method for the combined field integral equation, in *IEEE Antennas and Propagation Society International Symposium 2003*, vol. 3, pp. 543–546, IEEE Press, Piscataway, N. J.

F. Capolino, Dipartimento di Ingegneria dell'Informazione, Facoltà di Ingegneria, Via Roma, 56, Università di Siena, F-53100 Siena, Italy.

N.-W. Chen, Department of Electrical Engineering, National Central University, Chung-li, 32001, Taiwan.

M. Lu and E. Michielssen, Department of Electrical and Computer Engineering, University of Illinois at Urbana-Champaign, Urbana, IL 61801, USA. (mlu@emlab.uiuc.edu)

B. Shanker, Department of Electrical and Computer Engineering, Michigan State University, 2120 Engineering Building, East Lansing, MI 48824, USA.